1. Title page

Title

A new model measuring bacterial phagocytosis and phagolysosomal oxidisation in humans using the intradermal injection of methylene blue-labelled *Escherichia coli*

Author names and affiliations

George B Collins[1,2], Jhonatan de Souza Carvalho[1,3], Sandali C Jayasinghe[1], Urte Gumuliauskaite[1], David M Lowe[4], David C Thomas[5], Erik Årstad[6], Roel PH De Maeyer[7], Derek W Gilroy[1].

1. Department of Ageing, Rheumatology and Regenerative Medicine, Division of Medicine, University College London, London, UK.
2. Department of Cardiology, St Bartholomew's Hospital, Barts Health NHS Trust, London, UK.
3. Department of Diagnosis and Surgery, School of Dentistry, São Paulo State University (Unesp), São Paulo, Brazil.
4. Institute of Immunity & Transplantation, The Pears Building, University College London, London, UK.
5. Cambridge Institute of Therapeutic Immunology & Infectious Disease, Jeffrey Cheah Biomedical Centre, Cambridge Biomedical Campus, University of Cambridge, Cambridge, UK.
6. Centre for Radiopharmaceutical Chemistry, University College London, London, UK.

7. Botnar Research Centre, Nuffield Department of Orthopaedics, Rheumatology and Musculoskeletal Medicine, University of Oxford, Oxford, UK.

Corresponding author

- Derek W Gilroy, Department of Ageing, Rheumatology and Regenerative Medicine, Division of Medicine, Rayne Institute, University College London, 5 University St, London, WC1E 6JF. Email: d.gilroy@ucl.ac.uk

Conflict of interest statement

- The authors have no conflicts of interest to declare. All co-authors have seen and agree with the contents of the manuscript and there is no financial interest to report. We certify that the submission is original work and is not under review at any other publication.

2. Abstract

Phagocytosis is an important leucocyte function, however using existing models it cannot be measured in human tissues *in vivo*. To address this, we characterized a new phagocytosis model using intradermal methylene blue-labelled *Escherichia coli* injection (MBEC). Methylene blue (MB) is a licensed human medicine and bacterial stain potentially useful for labelling *E. coli* that are safe for human injection. *Ex vivo* co-culture of leucocytes with MBEC caused MB to transfer into neutrophils and macrophages by phagocytosis. During this, a 'red shift' in MB fluorescence was shown to be caused by phagolysosomal oxidisation. Hence, MBEC co-culture could be used to measure phagocytosis and phagolysosomal oxidisation in humans, *ex vivo*. In healthy volunteers,

inflammatory exudate sampling using suction blisters 2-24h after intradermal MBEC injection showed that tissue-acquired neutrophils and monocytes contained more MB than their circulating counterparts, whereas blood and inflamed tissue T, B and NK cells were MB^{lo}. This was validated with spectral flow cytometry by visualizing the MB emission spectrum in tissue-acquired neutrophils. Neutrophil MB emission spectra demonstrated more 'red shift' at 24h compared to earlier time-points, in-keeping with progressive phagolysosomal MB oxidisation in neutrophils over time *in vivo*. This new MBEC model can therefore measure bacterial phagocytosis and phagolysosomal oxidisation in human skin, *in vivo*. This has a number of important research applications, for example in studying human phagocyte biology, testing novel antimicrobials, and understanding why certain groups such as males, the elderly or those with diabetes, recent surgery or malnutrition are at increased risk of bacterial infection.

Keywords

Phagocytosis, infection, phagolysosomal oxidisation, human challenge models, neutrophils.

Summary sentence

This study characterized a new human challenge model to measure bacterial phagocytosis and phagolysosomal oxidisation in human skin *in vivo* using the intradermal injection of methylene blue-labelled *Escherichia coli*, followed by inflammatory exudate

sampling using suction blister formation and flow cytometry analysis of infiltrating leucocytes.

Main text

3. Introduction

Phagocytosis is an important leucocyte function, however there are no established experimental models that can measure this process in human tissues, *in vivo*.[1–3] This is important because tissues are the primary site of bacterial infection and phagocyte effector function, and many important phenotypic differences exist between circulating and tissue-acquired phagocytes.[4–9] As a result, previous studies of bacterial phagocytosis are restricted to *in silico* studies, murine models, and *ex vivo* culture of fluorescently-labelled particles with peripheral human blood leucocytes.[10–12] However, being performed outside the *in vivo* human body, these studies have limited translational capacity, which is hampering progress in our understanding of *in vivo* human phagocyte biology.[13–19]

The intradermal injection of ultraviolet (UV) light-killed *Escherichia coli* in humans is an established skin challenge model that generates a robust and self-resolving inflammatory response, and has provided important and novel insights into human *in vivo* immune responses.[20–24] Sampling inflammatory exudates by suction blister formation and drainage at different time-points after *E. coli* injection allows for temporal analysis of infiltrating leucocyte abundance and surface marker expression by flow cytometry. After human intradermal *E. coli* injection, professional phagocytes such as neutrophils and monocytes are the first and most abundant infiltrating leucocytes to migrate into the site

of inflammation, followed by adaptive immune cells such as lymphocytes and natural killer (NK) cells.[25] However, as the *E. coli* in this existing model are unlabelled, they cannot be used to measure phagocytosis in human skin, *in vivo*.

Methylene blue (MB) (Fig. 1) is a licensed human medicine and established bacterial stain that could be used to label UV-killed *E. coli* that are safe for human injection. MB-labelled *E. coli* (MBEC) could therefore be used to measure phagocytosis in humans *in vivo*. [26–28] Furthermore, because MB is a red-excited and red-emitting fluorophore, it is compatible with the detection range of both conventional and spectral flow cytometers.[29–31] MB-labelled *E. coli* (MBEC) could therefore be used alongside conjugated antibody staining of infiltrating dermal leucocytes to simultaneously measure their surface marker expression and phagocytic function in humans, *in vivo*.

This new model could overcome many of the translational limitations of existing *ex vivo* and murine phagocytosis models, and therefore has a number of important potential research applications. On that basis, we set out to characterize a new model to measure bacterial phagocytosis in human skin *in vivo* using the intradermal injection of methylene blue-labelled *E. coli* in healthy volunteers.

4. Methods

4.1 Ethics statement

For healthy volunteers, ethical approval was granted by the University College London Institutional Ethics Committee (ID: 1309/004), and for patients with chronic granulomatous disease (CGD) was provided by the local Health Research Authority

Research Ethics Committee (ID: 15/LO/1334). Volunteers provided written informed consent. All procedures were performed according to the 1975 Helsinki Declaration.

4.2 Recruitment

Unless otherwise stated, healthy, young (18-40 years), non-smoking volunteers of either sex and any ethnicity were recruited. Exclusion criteria were chronic inflammatory disease, recent illness, recent vaccination (≤3 months), routine blood test abnormalities, and any medication taken in the preceding week. Volunteers were required to refrain from alcohol and heavy exercise during the study.

4.3 Methylene blue

For *ex vivo* experiments, MB hydrate (*Sigma-Aldrich*) was diluted in phosphate buffered saline (PBS, *Gibco*) to the indicated concentration and filtered (*Whatman, 11μm*). For *in vivo* experiments, pharmaceutical grade 1% aqueous MB (*methylthioninium chloride*) was used instead (*FlexiPharm Austrading*). MB light absorbance was measured by spectrophotometry (*Tecan Spark*), and emission after red laser excitation during fluorescence microscopy (detection range 673-743nm) and flow cytometry. Spectrophotometry was performed with or without hydrogen peroxide (*LP Chemicals)* at the indicated concentrations.

The sensitivity of flow cytometric detection of MB was increased (i) using above-default detector voltages (AF647 = 650, AF700 = 650, APC-Cy7 = 600) with conventional flow

cytometry, (ii) using the 637nm detector at a voltage of 70 with spectral flow cytometry, and (iii) by merging the AF647, AF700, and APC-Cy7 channels *post hoc* using FCSExpress™ software (*De Novo*). In conventional flow cytometry, 'red shift' in neutrophil MB fluorescence was visualized by dividing the APC-Cy7 channel MFI by the AF647 channel MFI, and in spectral flow cytometry by dividing each data point on the MB emission curve by the sum of all data points for each condition. This corrects for differences in MB MFI between conditions and allows for side-by-side comparison of leucocyte MB emission spectra.

4.4 Preparation of human leucocytes and serum

Circulating leucocytes from the venous blood of healthy volunteers were sampled by venepuncture (*Greiner Bio-One*), anticoagulated with ethylenediaminetetraacetic acid (EDTA, *BD*), and isolated by diluting 1:10 with ACK lysis buffer (*Gibco*) for 6minutes (min) at room temperature (RT). Leucocytes were pelleted (*500g, 5min, RT*), washed in HBSS (*Gibco*), and resuspended in Roswell Park Memorial Institute 1640 medium (RPMI, *Gibco*) + 10% foetal calf serum (FCS, *Gibco*). To label leucocytes with MB, they were fixed in 2% paraformaldehyde (PFA, *ThermoFisher*), incubated in 1% MB in PBS for 60min, and washed in Hanks' Balanced Salt Solution (HBSS, *Gibco*). Neutrophils and monocytes were isolated by magnetic bead negative selection according to manufacturer's instructions using the EasySep™ and RosetteSep™ Isolation kits, respectively (*StemCell*). Monocytes were matured into monocyte-derived macrophages using 7-day culture in recombinant human macrophage colony-stimulating factor (50ng/ml, *Sigma-Aldrich*) at 37°C, before harvesting with ice-cold Accutase™ enzymatic

cell detachment media (*Invitrogen*). Autologous human serum was prepared from venous blood coagulated in serum separation tubes (*BD*) and isolated by centrifugation (*2000g, 10min, RT*).

4.5 Preparation of ultraviolet light-killed *Escherichia coli*

An antibiotic-sensitive strain of *E. coli* (*NCTC 10418*) from the UK Health Security Agency (formerly Public Health England) was cultured on Luria Bertani (LB) agar plates overnight at 37°C. A single colony forming unit (CFU) was transferred to a 10ml LB broth starter culture, incubated for 6h at 37°C, and 750µL transferred to 750ml LB broth for overnight incubation (*220rpm, 16h, 37°C*). The next morning, the broth was centrifuged (*4000g, 20min, 4°C*), washed twice in phosphate-buffered saline (PBS, *4000g, 20min, 4°C*), and sterilized for 2h with a 302nm ultraviolet (UV) light transilluminator (*UVP*). The UV-killed *E. coli* were then washed twice in sterile PBS (*4000g, 20min, 4°C*), and sterility was confirmed by the University College London Microbiology Laboratory, UK.

To quantify UV-killed *E. coli* at a wavelength of light absorbed by *E. coli* but not by MB, an optical density growth curve was generated using 420nm light (Fig. 2A). Aliquots of 1ml from the above 750ml culture broth were sampled and analysed every 30min. At each time-point, optical density at 420nm (OD_{420}) was measured, and CFUs were counted by serial dilution, overnight culture, colony counting, and dilution factor multiplication.

4.6 Labelling *Escherichia coli* with methylene blue

$5x10^8$ UV-killed *E. coli* in 2ml PBS were centrifuged (*6000g, 10min, RT*) in 2ml round-bottomed Eppendorfs (*Appleton Woods*) and the supernatant was removed. At a 60°

angle, pellets were labelled directly with 1µL 1% MB overnight at RT, resuspended in 2ml PBS, centrifuged (*6000g, 2min, RT*), and the washing solution removed. Where stated, 0.5% or 0.3% MB was used instead of 1% MB. MBEC pellets were resuspended in 200µL sterile 0.9% sodium chloride (NaCl) and quantified by OD_{420}. The quantity of MB attached to MBEC was calculated by increasing the concentration of pelleted *E. coli*, labelling with 1.3µL MB, and measuring the fall in MB concentration remaining in the MBEC washing solutions using the formula: mass = concentration x volume.

To assess the temporal stability of the MB label, MBEC were incubated at 37°C for 3h prior to flow cytometry. To confirm that their MB fluorescence originated from the labelled *E. coli* and not from their supernatants, the MB concentration of the labelling, washing, and final resuspension solutions were measured by spectrophotometry. For the same reason, amine non-reactive compensation beads (*Invitrogen*), which do not absorb MB, were resuspended in the final MBEC supernatants before flow cytometry.

4.7 Leucocyte co-culture with methylene blue-labelled *E. coli*

As part of a phagocytosis assay, neutrophils, monocytes, monocyte-derived macrophages, or all leucocytes were suspended in 10% autologous serum and co-cultured for 60min (unless stated otherwise) with either MBEC or unlabelled *E. coli* at the multiplicity of infection (MOI) provided. In all experiments, gated $SSC^{hi}FSC^{hi}$ granulocytes (of which ~95% are neutrophils) served as the unstained and single-stained controls for flow cytometry.[32] The flow cytometry gates separating MB^{lo} from MB^{hi} neutrophils (Supplemental Data 1) were defined using neutrophils co-cultured with unlabelled *E. coli* (i.e. a 'fluorescence-minus-one' control for MB). In some experiments, the above

phagocytosis assay was modified to answer different experimental questions. Therefore, where stated, neutrophils were (i) pre-treated with 10μM cytochalasin B in dimethylsulfoxide for 2h, (ii) supplemented with MB dye at the stated concentrations, or (iii) after MBEC co-culture resuspended in 100μL fixation-permeabilisation buffer (*eBioscience*).[33] To test the effect of MB on phagocytosis, pHrodo™ green *E. coli* BioParticles (*Invitrogen*) prepared in RPMI + 10% FCS according to the manufacturer's recommendations served as an alternative fluorescently-labelled particle to MBEC for measuring phagocytosis *ex vivo* (MOI = 20).

4.8 Flow cytometry

Before flow cytometry, leucocytes from the above assays were centrifuged (*500g, 5min, RT*), resuspended in 50μL of Brilliant Stain Buffer™ (*BD*) and 50μL of antibody solution (*30min, 4°C*), washed in FACS buffer (*500g, 5min, RT*), and fixed in 2% PFA (*ThermoFisher*). For conventional flow cytometry, the antibody solution contained FACS buffer and Live/dead Zombie UV™ (*BioLegend, 1:100*), CD45 BV785 (*BioLegend, 1:100*), CD3 PE dazzle (*BioLegend, 1:100*), CD19 BV605 (*BioLegend, 1:100*), CD56 BV605 (*BioLegend, 1:100*), CD4 PE-Cy7 (*BioLegend, 1:100*), CD8 BV510 (*BioLegend, 1:100*), HLA-DR BV421 (*BioLegend, 1:50*), CD66b FITC (*BioLegend, 1:50*), Siglec8 PE (*BioLegend, 1:50*), CD14 BUV805 (*BD, 1:100*), CD16 BUV395 (*BD, 1:100*), CD62L BUV737 (*BD, 1:100*) and CD45RA BV711 (*BioLegend, 1:100*). For spectral flow cytometry, the antibody solution contained FACS buffer and Live/dead Zombie UV (*BioLegend, 1:200*), CD45 SparkViolet538 (*BioLegend, 1:100*), CD3 PE (*BioLegend, 1:100*), CD19 PE (*BioLegend, 1:100*), HLA-DR PE (*BioLegend, 1:100*), CD56 PE

(*BioLegend, 1:100*), CD66b Pacific Blue (*BioLegend, 1:100*), Siglec8 BUV395 (*BD, 1:200*), CD11a FITC (*BioLegend, 1:200*), CD11b SparkBlue 550 (*BioLegend, 1:200*), CD14 SparkBlue 574 (*BioLegend, 1:200*), CD16 BV570 (*BioLegend, 1:200*), CD33 BUV496 (*BD, 1:200*), CD11c BV480 (*BD, 1:200*), CCR7 SparkYellowGreen 581 (*BioLegend, 1:200*), CD15 BUV563 (*BD, 1:200*), CD62L BV421 (*BioLegend, 1:200*), CXCR2 PE-Dazzle594 (*BioLegend, 1:200*), CXCR4 BV605 (*BioLegend, 1:200*). The gating strategy for each panel is shown in Supplemental data 1.

4.9 Fluorescence microscopy

For fluorescence microscopy single cell leucocyte suspensions were centrifuged (*800rpm, 5min, RT, Shandon Cytospin 2*) onto Polysine-coated microscope slides (*ThermoFisher*), fixed in 2% PFA for 10min, and washed twice in PBS. After 60min protein blockade in BlockAid™ solution (*Life Technologies*) leucocytes were stained with FITC-labelled anti-CD3, -CD14, -CD19, or -CD66b antibodies (*BioLegend*) for 60min at RT (*1:100*). Leucocytes were washed 3 times in PBS and mounted in ProLong™ Glass Antifade Mountant (*Invitrogen*) with or without Hoechst stain, before image acquisition at 63x magnification using oil-immersion fluorescence microscopy (*Leica TCS SP8*).

For live imaging, $2.5x10^4$ neutrophils were transferred to a chamber slide (*Thistle Scientific Ibidi*) containing 10% autologous serum. Image acquisition was performed every 6s with a *Zeiss LSM980 Airyscan* live imaging fluorescence microscope, 63x oil-immersion lens, and differential interference contrast (DIC) HSII Wollaston prism. Unlabelled *E. coli* or MBEC were added shortly after starting image acquisition (MOI = 100), which continued for 20min.

4.10 Skin model of acute inflammation

A 5cm^2 area of skin 7cm below the antecubital fossae on both volar forearms of healthy volunteers was shaved, marked, and cleaned (*Universal Alcotip*). 6x10^7 UV-killed *E. coli* or MBEC were prepared in sterile 0.9% NaCl as described above, and injected intradermally with a 1ml syringe (*BD*) and sterile 30G needle (*BD*). Dermal blood flow was measured by laser doppler imaging (*Moor Instruments*) and a skin biopsy or suction blister was performed at the pre-specified time-points as described below.

For skin biopsies, the site was cleaned with 2% chlorhexidine and anaesthetized with 2% lignocaine (*Hameln pharma*). A 5mm punch biopsy *(Stiefel*) was performed, cryopreserved in Optimum Cutting Temperature compound (OCT) *(VWR Chemicals*), cryosectioned at 50µM *(HM525 NX CryoStat*), and transferred to Polysine-coated microscope slides. Protein blockade, anti-CD66b staining, mounting, and image acquisition were performed as described above. The biopsy site was then cleaned, sutured, and covered, before the sutures were removed after 14 days.

For suction blisters, the host laboratory's technique was used, as previously described.[20] Briefly, a sealed cup with a 10mm aperture was connected to a negative pressure instrument (*Electronic Diversities NP-4*) and secured over the site of intradermal MBEC or *E. coli* injection. Suction was increased until a single epidermal blister filled the aperture. The negative pressure was then reduced, and the cup was removed. The blister roof was pierced with a sterile 18G needle (*BD*) and the exudate transferred to a 96-well plate (*ThermoFisher*) pre-filled with 50µL ice-cold 0.5µM EDTA in PBS. The blister was then deroofed, cleaned with 0.5% cetrimide (*Boots*), and covered with a sterile dressing (*Mepore)*. The inflammatory exudate was centrifuged (*1000g, 5min, 4°C*), and the blister

leucocytes stained with conjugated antibodies as described above. To measure blister fluid endotoxin levels (i.e. bacterial clearance), the cell-free exudate was diluted (*1:50*) in endotoxin-free LAL reagent water and analysed using the Endosafe NexGen™ portable endotoxin testing system (*Charles River*).

4.11 Data analysis and statistical calculations

At the default detector voltages (unless otherwise stated) conventional flow cytometry was performed using a *BD LSR Fortessa X20* and spectral flow cytometry using a *Sony ID7000 Spectral Cell Analyser*. For two-dimensional flow cytometry analysis, flow cytometry standard files were exported to *FlowJo* and numerical data to *GraphPad Prism*. For multi-dimensional flow cytometry analysis, $CD45^{hi}Lin^{lo}Siglec8^{lo}CD66b^{hi}$ neutrophils or $CD45^{hi}Siglec8^{lo}$ leucocytes (i.e. excluding $Siglec8^{hi}$ eosinophils) were imported to *R* and analysed using the referenced Cytof workflow.[34]

For statistical comparison, the means between 2 groups were compared with Student's *t*-tests and the means between 3 or more groups with one independent variable using one-way ANOVA and Dunnett's multiple comparisons test. The means between 3 or more groups with 2 independent categorical variables were compared with two-way ANOVA and Dunnett's multiple comparisons test. Statistical significance was shown as follows: *p ≤ 0.05, **p ≤ 0.01, ***p ≤ 0.001, ****p ≤ 0.0001, and ns = not significant.

5.0 Results

5.1 Methylene blue can be detected by fluorescence microscopy and flow cytometry

To begin developing a new *in vivo* phagocytosis model using the intradermal injection of methylene blue-labelled *E. coli* (MBEC), we first confirmed the excitation and emission wavelengths of MB. MB was maximally absorbent at 665nm (Fig. 2A) and hence maximally excited by the red laser (Fig. 2B). This was assessed using spectral flow cytometry (Fig. 2C) and fluorescence microscopy (Fig. 2D) by analysing the emission of fixed MB-labelled leucocytes after red laser excitation. Fixed leucocytes were used because in live cells MB is reduced to its transparent form leucocyte methylene blue, explaining its traditional use as a viability stain. At the default flow cytometry voltages, the best conventional flow cytometry channel to detect MB was the Alexa Fluor™ (AF) 647 channel (Fig. 2E), which combines red laser excitation with a 655-685nm detector set. Reserving the red laser exclusively for MB detection allowed simultaneous detection of 13 conjugated antibodies during conventional flow cytometry (see compensation matrix in Section 5.4), and 16 conjugated antibodies during spectral flow cytometry (Fig. 2F), in turn allowing multi-dimensional analysis of leucocyte surface marker expression alongside MB detection (Supplemental Data 1). Hence, alongside leucocyte surface molecule expression, MB could be detected after red laser excitation by flow cytometry and fluorescence microscopy.

5.2 Escherichia coli can be labelled with methylene blue

To measure phagocytosis *ex vivo,* we determined whether *E. coli* could be labelled with MB. Unlabelled antibiotic-sensitive *E. coli* were cultured overnight, killed with UV light, labelled with 1% MB, and washed in PBS. The concentration of MB in MB-labelled *E. coli* (MBEC) supernatants decreased from 1% during labelling, to $1x10^{-5}$ % after washing (Fig. 3A). Furthermore, when analysed by flow cytometry, labelled MBEC had significantly higher MB fluorescence than unlabelled *E. coli* (Fig. 3B).

To confirm that this MB fluorescence originated from the MBEC and not from any residual MB remaining in their supernatants after washing, MBEC geometric mean fluorescence intensity (MFI) was compared to amine non-reactive beads suspended in the same MBEC supernatants. These amine non-reactive beads are similar in size to *E. coli*, but do not bind organic dyes such as MB. MBEC had significantly higher MB fluorescence than the beads, suggesting that the MB fluorescence in the MBEC originated from the labelled bacteria and not from their supernatants (Fig. 3C). Next, MBEC were incubated in culture medium for 3h. During this time, they did not lose their MB label (Fig. 3D), showing that the MB labelling of UV-killed *E. coli* was stable over time.

To calculate the amount of MB attached to *E. coli* and therefore whether the MB label could affect immune responses, the quantity of MB attached to MBEC was inferred from the concentration of MB remaining in the washing solution after labelling increasing quantities of UV-killed *E. coli* with the same volume of 1% MB. The amount of MB bound to the labelled *E. coli* was in the order of picograms (Fig. 3E), 11 orders of magnitude below the intravenous dose of MB used in clinical practice (1-2mg/kg) for the treatment of conditions such as acquired methaemaglobinaemia.[35,36]

Before intradermal MBEC injection, accurate bacterial quantification was also important. However, UV-killed *E. coli* are usually quantified using spectrophotometry at OD_{600}, a wavelength of light that is absorbed by MB (Fig. 2A).[37] Therefore, to infer MBEC concentration independent of MB-labelling, a new standard curve (Fig. 3F) was generated using OD_{420}, a wavelength of light absorbed by *E. coli* (Fig. 3G) but not by MB (Fig. 2A). Hence, UV-killed *E. coli* could be labelled with MB, washed, and accurately quantified.

5.3 Methylene blue-labelled *Escherichia coli* can be used to measure phagocytosis *ex vivo*

To understand whether MBEC could be used to measure bacterial phagocytosis *ex vivo*, circulating leucocytes from healthy volunteers were co-cultured with MBEC or unlabelled *E. coli*, stained with conjugated antibodies, and analysed by flow cytometry. Co-culture of leucocytes with MBEC caused MB to transfer primarily into neutrophils (Fig. 4A). The absence of MB in the other less phagocytic leucocyte subsets suggested that this transfer was caused by phagocytosis, and not by diffusion of any residual MB remaining in the MBEC supernatants. This was supported when the MB fluorescence of neutrophils during incubation with MBEC increased over time (Fig. 4B) and with increasing multiplicity of infection (MOI, Fig. 4C), but not with unlabelled *E. coli* controls (Fig. 4D).

This was further supported when (i) cytochalasin B pre-treatment (which inhibits phagocytosis) reduced MB transfer into neutrophils (Fig. 4D), (ii) MB uptake was higher in monocyte-derived macrophages than naïve circulating monocytes (Figure 4E), and (iii) the leucocyte staining pattern after MBEC co-culture (Fig. 4F) was different to after direct labelling of fixed leucocytes with MB dye (Fig. 2D).[33] Specifically, the leucocytes co-

cultured with MBEC contained MB^{hi} inclusions resembling phagolysosomal staining, but direct labelling of fixed leucocytes with MB produced nuclear staining, suggesting that staining during MBEC co-culture was caused by phagocytosis and not by the diffusion of MB into leucocytes from MBEC supernatants.[38–42] Staining leucocytes after MBEC co-culture with conjugated antibodies confirmed that these MB^{hi} inclusions (Fig. 4F) were absent after co-culture with unlabelled *E. coli*, primarily observed in neutrophils, and present to a lesser extent in naïve circulating monocytes (Fig. 4G).

The hypothesis that MBEC phagocytosis caused these MB^{hi} inclusions was confirmed by the live microscopy imaging videos in Supplemental Data 2 and still image frames from these videos in Fig. 4H. During MBEC co-culture, neutrophils internalized MBEC, forming intracellular and non-nuclear MB^{hi} inclusions in-keeping with phagolysosomal staining (Supplemental data 2B).[38–42] Again, these inclusions were different from direct staining of fixed leucocytes with MB (Fig. 2D), and absent during co-culture with unlabelled *E. coli* (Supplemental Data 2A and Fig. 4H).

When neutrophils were treated with membrane permeabilisation buffer after co-culture with MBEC, MB fluorescence was significantly reduced (Fig. 3I). This was likely due to dissipation of MB through perforated phagolysosomal and extracellular membranes, further supporting the value of MBEC in measuring bacterial phagocytosis. Finally, when neutrophils were co-cultured with either MBEC or pH-sensitive pHrodo™ green *E. coli* BioParticles at an equivalent MOI (20), both MB and pHrodo™ green dye accumulated in neutrophils at an equivalent rate (Fig. 4J).

Together, these data suggested that MBEC were equally effective to a commercial fluorescent probe in measuring phagocytosis *ex vivo,* whilst also being safe for human injection.

5.4 Methylene blue-labelled *Escherichia coli* can also measure phagolysosomal oxidisation *ex vivo*

Because the red emission spectrum of MB (Fig. 2B) was wider than the detection range of the AF647 flow cytometry channel (655-685nm), using the AF647 channel alone to detect MB excluded the red-emitting MB fluorescence outside this range, reducing the sensitivity of conventional flow cytometry to MB. To address this, fluorescence data from the AF647 channel (655-685nm) was combined with the AF700 (705-750nm) and APC-Cy7 channels (750-810nm) *post hoc* using FCS Express™ software, a novel concept not previously described in the literature. This created a merged, virtual 'MB channel', with the wider detection range 655-810nm, increasing the amount of gathered light and therefore sensitivity of conventional flow cytometry to MB (benefitted because cellular autofluorescence is low at these wavelengths). This was supported by the MFI data in Fig. 5A, which shows the AF647, AF700, APC-Cy7 and merged 'MB channel' MFIs for neutrophils during 60min MBEC co-culture. Despite this wider detection range, combining detection of neutrophil MB (i.e. phagocytosed MBEC) with 13 conjugated antibody fluorophores still produced satisfactory overlap values during conventional flow cytometry fluorophore compensation (Fig. 5B).

During analysis of these 3 red emission-detecting conventional flow cytometry channels, we noticed that *ex vivo* MBEC phagocytosis caused the emission spectrum of MB in

neutrophils to 'shift' from the near-red AF647 channel towards the far-red APC-Cy7 channel (Fig. 5A and C). Hereafter referred to as 'red shift', this change in MB emission from the near-red to the far-red side of the light spectrum was quantified by dividing the far-red APC-Cy7 channel MFI by the near-red AF647 MFI to generate an APC-Cy7:AF647 ratio (Fig. 5D). This 'red shift' was confirmed using spectral flow cytometry to be caused by a fall in the 696nm primary emission peak, and an increase in the 760nm shoulder emission peak during MBEC phagocytosis (Fig. 5E).

We next investigated the cause of this 'red shift' in MB emission during MBEC phagocytosis, with the hypothesis that it could be caused by phagolysosomal oxidisation, an important bactericidal process in neutrophils.[43] To test this, we combined MB with increasing concentrations of hydrogen peroxide (H_2O_2) *in vitro*, and observed a noticeable 'red shift' in MB fluorescence (Fig. 5F and G).

To assess whether this 'red shift' was caused by phagolysosomal oxidisation *ex vivo*, MBEC were co-cultured with neutrophils from patients with X-linked (gp91phox) chronic granulomatous disease (CGD), who due to defective nicotinamide adenine dinucleotide phosphate oxidase activity cannot effectively oxidize their phagolysosomes.[44] Despite similar phagocytic capacity between neutrophils from CGD patients and healthy controls (Fig. 5H), the 'red shift' in MB fluorescence during MBEC phagocytosis was absent in CGD patients, with female carriers manifesting an intermediate phenotype consistent with lyonization of the abnormal X chromosome in approximately 50% of neutrophils (Fig. 5I and J). This suggested that the 'red shift' in neutrophil MB emission observed during MBEC phagocytosis was caused by phagolysosomal oxidisation and not by MB accumulation. This was confirmed when the 'red shift' in MB fluorescence persisted

despite reducing the concentration of MB used to label the UV-killed *E. coli* prior to neutrophil MBEC co-culture from 1% to 0.5% and 0.3% (Fig. 5K). Together, these data showed that in addition to bacterial phagocytosis, MBEC can also be used to independently measure phagolysosomal oxidisation in humans *ex vivo.*

5.5 Inflammation caused by methylene blue-labelled *Escherichia coli* is similar to that caused by unlabelled *E. coli*

Having demonstrated that MBEC can be used to measure phagocytosis and phagolysosomal oxidisation *ex vivo*, we next compared the immune response between MBEC and unlabelled *E. coli*. This was to understand whether MBEC were equally inflammatory to the unlabelled *E. coli* used in the existing skin challenge model, and whether MB labelling had any immunomodulatory effect on the pattern of acute inflammation *in vivo.* Neutrophils co-cultured with MBEC *ex vivo* showed equivalent changes in activation status to those co-cultured with unlabelled *E. coli*, whereby CD11b, CD45, and CD66b were upregulated (Fig. 6A, B and D, respectively), and CD62L was shed (Fig. 6C).

The functional effect of MB on bacterial phagocytosis was then tested using pHrodo™ green *E. coli* BioParticles, which are detected in the FITC channel and therefore do not spectrally overlap with MB (Fig. 2E and 5B). MB dissolved in the phagocytosis assay culture medium inhibited pHrodo™ green *E. coli* BioParticle phagocytosis by neutrophils at MB concentrations above $1x10^{-3}$% (Fig. 6E), however this was 2 orders of magnitude over the MB concentration present in MBEC supernatants (Fig. 3A).

To replicate the MBEC model more closely, the effect of MB as an *E. coli* label on phagocytosis was then tested by measuring phagocytosis of pHrodo™ green *E. coli* BioParticles in combination with increasing concentrations of either MBEC or unlabelled *E. coli*. When used as an *E. coli* label, MB inhibited phagocytosis at an MOI of over 500, 3 orders of magnitude above the MOI present in human skin after intradermal *E. coli* injection (Fig. 6F).[45]

Having demonstrated that at the concentrations present in the MBEC model MB had little effect on neutrophil function *ex vivo*, the effect of MB on acute inflammation was investigated in humans *in vivo.* MBEC and unlabelled *E. coli* were injected intradermally into the left and right volar forearms of healthy volunteers, respectively. Laser doppler imaging showed that the increase in blood flow after intradermal MBEC injection was similar to after unlabelled *E. coli* injection (Fig. 6G). Dermal neutrophil infiltration rates were also similar between MBEC and unlabelled *E. coli* injections (Fig. 6H and Supplemental Data 3A-B). Finally, after bilateral intradermal MBEC injections, the vascular hyperaemia, systemic neutrophilia, and sequential waves of myeloid and then lymphoid leucocyte infiltration were also similar to other published studies using unlabelled *E. coli* injection in humans (Fig. 6I-K and Supplemental Data 3C).[20–23] Importantly, no adverse events were reported after intradermal MBEC injection in healthy volunteers. Hence, the addition of a MB label to the existing intradermal *E. coli* model was safe, and had no effect on neutrophil function or acute inflammation.

5.6 Methylene blue-labelled *Escherichia coli* can measure phagocytosis in human skin during the onset of inflammation

Having shown that (i) *E. coli* can be stably labelled with MB, (ii) phagocytosis of MBEC can be measured *ex vivo,* and (iii) MBEC can be safely injected intradermally into healthy volunteers to cause inflammation that is similar to after unlabelled *E. coli* injection, we next investigated whether MBEC could be used to measure phagocytosis in human skin, *in vivo.* Mouse models were not required because (i) numerous fluorescently labelled particles to measure phagocytosis in mouse models are already commercially available, (ii) the safety of intradermal unlabelled *E. coli* injection in humans is already well-established, and (iii) the quantity of MB attached to killed *E. coli* was negligible compared to the doses used in clinical practice (Fig. 3E).

Because neutrophils first appeared in human skin biopsies 2-3h after intradermal MBEC injection (Fig. 6H), leucocytes were sampled from dermal suction blisters and the venous blood of healthy volunteers at this time-point. Due to their primed $CD66b^{hi}CD11b^{hi}CD45^{hi}CD62L^{lo}$ expression profile, blister neutrophils clustered separately to blood neutrophils during unsupervised UMAP analysis. This showed that they were an extravasated and tissue-derived phenotype, and not a haemorrhagic contaminant produced as a by-product of the blistering process (Fig. 7A and B). In-keeping with this, blister neutrophils were also MB^{hi} compared to blood neutrophils (Fig. 7B and C), demonstrating that MB accumulated in neutrophils locally at the site of MBEC injection rather than through systemic dissemination. This suggested that intradermal MBEC injection could be used to measure bacterial phagocytosis in human skin, *in vivo*. To examine this in more detail, blood neutrophils were excluded from the analysis. During unsupervised UMAP analysis the remaining blister neutrophils separated into 3 clusters of increasing MB fluorescence (Fig. 7D). This again suggested that intradermal MBEC

injection could be used to measure phagocytosis in human skin *in vivo*, and also that the transfer of MB into neutrophils was not caused by diffusion, which would otherwise cause MB to distribute equally into all neutrophils. MB^{lo} blister neutrophils (Cluster 1) in this analysis (Fig. 7D, E and F) were therefore likely to be an infiltrating phenotype, that had extravasated but not yet phagocytosed MBEC. This was supported when the bacterial receptors CD11b, CD66b, CD14, and CD16 were all lower expressed in MB^{hi} blister neutrophils (Cluster 3) compared to the MB^{int} (Cluster 2) and/or MB^{lo} (Cluster 1) blister neutrophil clusters (Fig. 7D, E and F), in-keeping with progressive pathogen-receptor internalisation during *in vivo* MBEC phagocytosis.[46,47] In summary, these data suggested that 2-3h after intradermal injection (i.e. during the onset phase of acute inflammation), MBEC could be used to measure bacterial phagocytosis in human skin, *in vivo*.

5.7 Methylene blue-labelled *Escherichia coli* can measure phagocytosis in human skin *in vivo* during the resolution phase of acute inflammation

We then extended this model to investigate whether MBEC could be used to measure phagocytosis *in vivo* in healthy volunteers at later timepoints after intradermal injection (i.e. at 3h, 5h, 7h, 9h and 24h). 19 volunteers underwent bilateral MBEC injection and suction blister formation, each person contributing to the timecourse dataset either (i) a 3h and 5h blister, (ii) a 7h and 9h blister, or (iii) two 24h blisters (38 data points, n = 7/8 per time-point). In-keeping with inflammation onset and then resolution, the number of blister neutrophils peaked at 9h, but by 24h had fallen to around 1000 cells per blister (Supplemental Data 3C). At these later phase timepoints, blood and blister neutrophils again clustered separately during UMAP analysis (Fig. 8A). Blister neutrophils were also

MB^{hi} compared to blood neutrophils (Fig. 8B and C), even more so than in blister neutrophils sampled during inflammation onset (Fig. 7C). This was supported by visualisation of the MB emission spectrum in blister neutrophils when analysed by spectral flow cytometry (Fig. 8D), which also confirmed that neutrophil MB MFI was not caused by increase in neutrophil autofluorescence during the extravasation process.

Further in-keeping with this model being able to measure MBEC phagocytosis *in vivo*, the MB MFI of blister neutrophils (Fig. 8E) and MB^{hi} blister neutrophil abundance (Fig. 8F) both increased over time. In addition, the total MB fluorescence in all blister neutrophils (MB MFI x neutrophil count = MB fluorescence intensity) increased alongside the fall in blister exudate bacterial endotoxin levels (i.e. bacterial clearance from the extracellular space, Fig. 8G). Together, these data suggested that after intradermal MBEC injection, the MBEC model could also identify when bacterial clearance was complete, and therefore the exact onset of inflammatory resolution.

The hypothesis that intradermal MBEC injection could be used to measure phagocytosis in humans *in vivo* was further supported when the statistical correlations between MB MFI and expression of the other neutrophil surface molecules were the same whether neutrophils were sampled from the *in vivo* MBEC model (i.e. after intradermal MBEC phagocytosis) or from an *ex vivo* phagocytosis assay (Fig. 8H). Put simply, the observation that both *in vivo* and *ex vivo* MBEC phagocytosis caused similar changes in neutrophil surface marker expression suggested that MB uptake in both contexts was caused by the same process (i.e. by MBEC phagocytosis).

This was further supported when the MB in 24h blister neutrophils exhibited more 'red shift' than blister neutrophils from earlier time-points (Fig. 8I), in-keeping with progressive

MB phagolysosomal oxidisation in infiltrating neutrophils over time (Figure 5E). This, in turn, suggested that, in addition to bacterial phagocytosis, intradermal MBEC injection could also be used to measure phagolysosomal oxidisation in human skin, *in vivo*.

Finally, an unsupervised UMAP analysis of all blood and blister leucocyte subtypes after intradermal MBEC injection (excluding Siglec8^{hi} eosinophils, Fig. 9A) showed that, in addition to neutrophils, blister monocytes were also MB^{hi} compared to their circulating counterparts (Fig. 9B and C), and blood and blister T, B, and NK cells were MB^{lo}. The exclusive presence of MB in the phagocytic dermal leucocyte subsets further suggested that this new MBEC model could indeed be used to measure bacterial phagocytosis in human skin, *in vivo*.

Together, these data show that UV-killed *E. coli* can be labelled with MB, safely injected into the skin of healthy volunteers, and used to measure both phagocytosis and phagolysosomal oxidisation during both inflammation onset and its resolution.

6. Discussion

These results show that UV-killed *E. coli* could be labelled with methylene blue (MB), injected into the skin of healthy volunteers, and used to measure phagocytosis in human skin, *in vivo*. In parallel, infiltrating leucocyte abundance and surface molecule expression could be measured by detecting conjugated antibody staining alongside MB fluorescence. Finally, during phagocytosis of methylene blue-labelled *E. coli* (MBEC), phagolysosomal oxidisation caused a 'red shift' in neutrophil MB fluorescence. Hence, after a single intradermal MBEC injection, bacterial phagocytosis and phagolysosomal oxidisation could, for the first time, be measured in human tissues, *in vivo*. This, in turn, allowed

dermal MB^{lo} infiltrating neutrophils to be distinguished from MB^{hi} phagocytosing neutrophils, and also accurate identification of the end of bacterial clearance, and hence the onset of inflammatory resolution.

The majority of bacterial infections occur in epithelial tissues, primarily the skin, lungs, intestines, and genitourinary tract.[48,49] This model is the first to measure bacterial phagocytosis in human tissues, *in vivo*.[45,50] The use of MB as a bacterial stain depends on its overall positive charge, which originates from the quaternary amine in its molecular structure.[51–53] This allows MB to bind to anions such as DNA, RNA, LPS, and glycoproteins, in turn explaining its nuclear staining pattern in fixed MB-labelled leucocytes (Fig. 2D).[54–56] An alternative label to MB could be the recently developed fluorescently-labelled antibiotic 7-nitrobenz-2-oxa-1,3-diazole-labelled ubiquicidin, which, albeit having a less well-established safety profile compared to MB, is also safe for human injection.[57,58] However, having been designed to visualise free bacteria in the human lung *in vivo*, its stability during phagocytosis, and therefore its response to phagolysosomal oxidisation, has not been established.

The only existing model capable of measuring phagocytosis at the cellular level in humans *in vivo* uses synthetic skin chambers placed on top of the exposed dermis, which is uncovered by deroofing suction blisters raised on the naïve skin of healthy volunteers.[50] In this model, neutrophils are recruited into the skin chambers using autologous serum, before fluorescein-labelled heat-killed *E. coli* are added to measure phagocytosis in extravasated neutrophils.[50] However, being a non-resolving model, this skin chamber technique does not generate the sequential waves of neutrophils, monocytes, and lymphocytes seen in the self-resolving MBEC model. It therefore cannot be used to

measure monocyte phagocytosis, infer innate-adaptive immune cell interactions, or investigate the non-phagocytic roles of myeloid cells during the resolution phase of acute inflammation.[50,59–63] Furthermore, the existing skin chamber technique measures phagocytosis in solution and on the dermal surface, and not within the skin tissue architecture.[50] It is therefore more similar to an *ex vivo* phagocytosis assay using primed neutrophils than to true *in vivo* phagocytosis, which as mentioned is usually parenchymal. In contrast, by using bacteria as the sole inflammatory stimulus, and sampling leucocytes from within the dermal interstitium, the MBEC model is more physiological, and more closely resembles an actual self-limiting bacterial skin infection.

Another disadvantage of the existing skin chamber model is that fluorescein is quenched under acidic conditions, such as those found in the maturing phagolysosome.[64,65] In contrast, MB is stable under acidic conditions, and during the current investigation remained fluorescent throughout MBEC phagocytosis.[66,67] The well-recognized photostability of MB derives from the ability of delocalized electrons in its planar aromatic rings to dissipate absorbed light energy and become stabilized by protonation (Fig. 1), as also occurs within the maturing phagolysosome.[68–72] In-keeping with this, the relatively few blister neutrophils present 24h after intradermal MBEC injection still contained MB. Although interpreting intravital stains is increasingly challenging at later time-points post-injection, this was supported by the well-recognised anti-apoptotic effects of neutrophil migration into sites of inflammation, and also by the observations from a three-dimensional *ex vivo* phagocytosis assay scaffold, which showed that neutrophils still contained labelled bacteria 16h after phagocytosis.[73]

The ability of the MBEC model to measure phagolysosomal oxidisation shows not only that MBEC are a fluorescently-labelled particle capable of initiating inflammation and measuring phagocytosis, but also that in this context MB is a ratiometric dye sensitive to phagolysosomal oxidisation. Combining a ratiometric dye with conjugated antibody staining and flow cytometry is a relatively new concept, recently described using Fluorescence Resonance Energy Transfer dyes, which are typically used to study protein-protein interactions *ex vivo*.[74–76]. Using a single label as both a fluorescent probe and a ratiometric dye is a useful approach in human *in vivo* model design, as it increases information yield (and therefore discovery potential) without the additional risk to participants of a second particle or injection.

Another unavoidable limitation of intravital staining is that the injected dye can affect the function it is designed to measure. However, in the current investigation, compared to unlabelled *E. coli*, intradermal MBEC injection did not affect the hyperaemic response to bacterial injection, *in vivo*. Furthermore, MB did not affect *ex vivo* phagocytosis, at least not until the MB concentration was increased to $1x10^{-3}$ % (2 orders of magnitude above that in MBEC supernatants), or until the MBEC MOI was increased to $1x10^{3}$ (3 orders of magnitude above that found in humans after intradermal UV-killed *E. coli* injection).[45] This is supported by a recent study by Trevisan *et al*, who showed that neutrophil phagocytosis of *Candida albicans* was unaffected by $1x10^{-2}$ % MB.[77] Three studies have shown that after spinal cord or lung injury in rats, MB reduces neutrophil migration into sites of inflammation.[78–80] However, the doses of MB used in these studies was 11 orders of magnitude over those present in MBEC supernatants in our experiments. This was supported in the current investigation when neutrophil infiltration was similar between

intradermal unlabelled *E. coli* and MBEC injections. Hence, although the effects of MB on leucocyte migration were not formally tested *ex vivo*, at the MB concentrations used in the MBEC model, MB is highly unlikely to affect neutrophil phagocytosis or infiltration in human skin, *in vivo*.

This new model has several important potential applications. In basic research, it could help understand how bacterial uptake is divided between the phagocyte subtypes, the role of non-phagocytic myeloid cell subtypes, and whether the previously identified differences between neutrophil and monocyte phagolysosomal oxidisation *ex vivo* are also present *in vivo*.[81–84] Furthermore, by separating early-arriving MB^{lo} 'infiltrating', MB^{hi} 'phagocytosing', and late-arriving MB^{lo} 'resolution-phase' phagocytes, the MBEC model could help inform studies investigating leucocyte extravasation and the non-canonical roles of phagocytic leucocytes during inflammation onset and its resolution.

In translational research, the MBEC model could explain why some people are at higher risk of bacterial infection, such as males, the elderly, or patients with recent surgery, diabetes mellitus, or malnutrition.[85–87] In clinical research, it could help clarify whether new or existing therapies can accelerate phagocytosis *in vivo*, whether defective phagocyte function is the cause of unexplained immunodeficiency, or why some therapies, such as corticosteroids, predispose to infection.[88,89]

The current investigation could also serve as a roadmap for the development of similar human challenge models, designed to answer different experimental questions. For example, labelling *E. coli* with other clinically safe dyes (e.g. indocyanine green, rose Bengal, or acriflavine), which have their own unique fluorescent properties, and therefore potential research applications. Alternatively, labelling different bacterial species (e.g.

Staphylococcus aureus) with MB could help investigate species-specific differences in phagocytosis and phagolysosomal oxidisation in human skin, *in vivo*.[90–92]

In addition to those already mentioned, one limitation of the MBEC model is its incompatibility with cell membrane permeabilisation, and therefore with intracellular antibody staining. This is likely due to surface and phagolysosomal membrane disruption caused by permeabilisation, which result in MB dissolution. This precludes phagocytosis measurement in myeloid cell sub-types that are only identifiable by their intracellular molecule expression.[93]

Another limitation is that since naïve skin is largely devoid of neutrophils, in the MBEC model blister neutrophil MB MFI is affected by leucocyte infiltration rate.[94,95] Put simply, early-infiltrating or fast-moving neutrophil populations are likely to contain more MB as they have had more time to phagocytose MBEC at a time closer to the MBEC injection, when more bacteria are present and therefore available for phagocytosis. This makes direct comparison of the phagocytic capacity of different leucocyte subtypes between time-points during the inflammatory response more complex, as their MB MFI is also dependent on their rate of infiltration into, and time of arrival at, the site of MBEC injection. However, this is an unavoidable by-product of the self-resolving and inherently physiological nature of the new MBEC model, which itself is accompanied by the advantages already described above.

In conclusion, this study showed that the intradermal injection of methylene blue-labelled *E. coli*, followed by suction blister formation and flow cytometry analysis of infiltrating leucocytes, can measure bacterial phagocytosis and phagolysosomal oxidisation in human tissues, *in vivo*. This new model is the first of its kind and has a number of

important potential research applications that could significantly improve our understanding of the immune response to bacterial infection in humans, *in vivo*.

7. Acknowledgments and Funding Sources

This research was supported by the Wellcome Trust, grant number 554737 (175479) and the UCL Centre for Radiopharmaceutical Chemistry (CRC), which is funded in part by the NIHR UCLH BRC.

The authors would like to thank all the participants who volunteered for the study, Flexipharm Austrading who donated the clinical grade methylthioninium chloride (methylene blue), and finally the following colleagues for their invaluable support and advice throughout the project: Larissa Benvenutti, Joseph Boyle, Olivia Bracken, Jeremy Brown, Jamie Evans, Karen Feehan, James Glanville, Alan Greig, Samantha Palethorpe, Michael Redd, and Michelle Sugimoto.

8. Authorship Contribution Statement

GC, RDM, EA, and DG conceptualized the study. GC, JC, SJ, and UG performed the investigation. GC performed data curation and analysis. GC wrote the original draft. GC, JC, SJ, UG, RDM, DL, DT, EA, and DG were responsible for reviewing, editing, and revising the manuscript.

9. References

1. Bicker H, Höflich C, Wolk K, Vogt K, Volk H-D, Sabat R. A Simple Assay to Measure Phagocytosis of Live Bacteria. Clinical Chemistry. 2008;54(5):911–915. https://doi.org/10.1373/clinchem.2007.101337

2. Hampton MB, Winterbourn CC. Methods for quantifying phagocytosis and bacterial killing by human neutrophils. Journal of Immunological Methods. 1999;232(1–2):15–22. https://doi.org/10.1016/s0022-1759(99)00147-7

3. Gu BJ, Sun C, Fuller S, Skarratt KK, Petrou S, Wiley JS. A quantitative method for measuring innate phagocytosis by human monocytes using real-time flow cytometry. Cytometry Part A. 2014;85(4):313–321. https://doi.org/10.1002/cyto.a.22400

4. Fortunati E, Kazemier KM, Grutters JC, Koenderman L, Van den Bosch VJMM. Human neutrophils switch to an activated phenotype after homing to the lung irrespective of inflammatory disease. Clinical and Experimental Immunology. 2009;155(3):559–566. https://doi.org/10.1111/j.1365-2249.2008.03791.x

5. Arve-Butler S, Schmidt T, Mossberg A, Berthold E, Gullstrand B, Bengtsson AA, Kahn F, Kahn R. Synovial fluid neutrophils in oligoarticular juvenile idiopathic arthritis have an altered phenotype and impaired effector functions. Arthritis Research and Therapy. 2021;23(1):1–12. https://doi.org/10.1186/s13075-021-02483-1

6. Moonen CGJ, Hirschfeld J, Cheng L, Chapple ILC, Loos BG, Nicu EA. Oral Neutrophils Characterized: Chemotactic, Phagocytic, and Neutrophil Extracellular Trap (NET) Formation Properties. Frontiers in Immunology. 2019;10. https://doi.org/10.3389/fimmu.2019.00635

7. Davidsson L, Björkman L, Christenson K, Alsterholm M, Movitz C, Thorén FB, Karlsson A, Welin A, Bylund J. A simple skin blister technique for the study of in vivo transmigration of human leukocytes. Journal of Immunological Methods. 2013;393(1–2):8–17. https://doi.org/10.1016/j.jim.2013.03.013

8. Metzemaekers M, Malengier-Devlies B, Yu K, Vandendriessche S, Yserbyt J, Matthys P, De Somer L, Wouters C, Proost P. Synovial Fluid Neutrophils From Patients With Juvenile Idiopathic Arthritis Display a Hyperactivated Phenotype. Arthritis and Rheumatology. 2021;73(5):875–884. https://doi.org/10.1002/art.41605

9. Briheim G, Coble B, Stendahl O, Dahlgren C. Exudate polymorphonuclear leukocytes isolated from skin chambers are primed for enhanced response to subsequent stimulation with chemoattractant f-Met-Leu-Phe and C3-opsonized yeast particles. Inflammation. 1988;12(2):141–152. https://doi.org/10.1007/BF00916397

10. Lehmann AK, Sørnes S, Halstensen A. Phagocytosis: Measurement by flow cytometry. Journal of Immunological Methods. 2000;243(1–2):229–242. https://doi.org/10.1016/s0022-1759(00)00237-4

11. Chow C, Downey GP, Grinstein S. Measurements of Phagocytosis and Phagosomal Maturation. Curr Protoc Cell Biol. 2004 May;Chapter 15:Unit 15.7. https://doi.org/10.1002/0471143030.cb1507s22

12. Platt N, Fineran P. Measuring the phagocytic activity of cells. Methods Cell Biol. 2015;126:287-304. https://doi.org/10.1016/bs.mcb.2014.10.025

13. McGonigle P, Ruggeri B. Animal models of human disease: Challenges in enabling translation. Biochemical Pharmacology. 2014;87(1):162–171. https://doi.org/10.1016/j.bcp.2013.08.006

14. Coughlan AM, Freeley SJ, Robson MG. Humanised mice have functional human neutrophils. Journal of Immunological Methods. 2012;385(1–2):96–104. https://doi.org/10.1016/j.jim.2012.08.005

15. Hasenberg A, Hasenberg M, Männ L, Neumann F, Borkenstein L, Stecher M, Kraus A, Engel DR, Klingberg A, Seddigh P, et al. Catchup: a mouse model for imaging-based tracking and modulation of neutrophil granulocytes. Nature Methods. 2015;12(5):445–452. https://doi.org/10.1038/nmeth.3322

16. Zheng Y, Sefik E, Astle J, Karatepe K, Öz HH, Solis AG, Jackson R, Luo HR, Bruscia EM, Halene S, et al. Human neutrophil development and functionality are enabled in a humanized mouse model. Proceedings of the National Academy of Sciences. 2022;119(43). https://doi.org/10.1073/pnas.2121077119

17. Dyson A, Singer M. Animal models of sepsis: Why does preclinical efficacy fail to translate to the clinical setting? Critical Care Medicine. 2009;37(Supplement):S30–S37. https://doi.org/10.1097/ccm.0b013e3181922bd3

18. Brubaker DK, Lauffenburger DA. Translating preclinical models to humans. Science. 2020;367(6479):742–743. https://doi.org/10.1126/science.aay8086

19. Koboziev I, Jones-Hall Y, Valentine JF, Reinoso Webb C, Furr KL, Grisham MB. Use of Humanized Mice to Study the Pathogenesis of Autoimmune and Inflammatory Diseases. Inflammatory Bowel Diseases. 2015;21(7):1652–1673. https://doi.org/10.1097/mib.0000000000000446

20. Motwani MP, Flint JD, De Maeyer RPH, Fullerton JN, Smith AM, Marks DJB, Gilroy DW. Novel translational model of resolving inflammation triggered by UV-killed E. coli.

Journal of Pathology: Clinical Research. 2016;2(3):154–165. https://doi.org/10.1002/cjp2.43

21. Motwani MP, Newson J, Kwong S, Richard-Loendt A, Colas R, Dalli J, Gilroy DW. Prolonged immune alteration following resolution of acute inflammation in humans. PLoS ONE. 2017;12(10):1–16. https://doi.org/10.1371/journal.pone.0186964

22. Motwani MP, Colas RA, George MJ, Flint JD, Dalli J, Richard-Loendt A, De Maeyer RP, Serhan CN, Gilroy DW. Pro-resolving mediators promote resolution in a human skin model of UV-killed Escherichia coli-driven acute inflammation. JCI insight. 2018;3(6):1–14. https://doi.org/10.1172/jci.insight.94463

23. Maini AA, George MJ, Motwani MP, Day RM, Gilroy DW, O'Brien AJ. A comparison of human neutrophils acquired from four experimental models of inflammation. PLoS ONE. 2016;11(10):1–15. https://doi.org/10.1371/journal.pone.0165502

24. Motwani MP, Bennett F, Norris PC, Maini AA, George MJ, Newson J, Henderson A, Hobbs AJ, Tepper M, White B, et al. Potent Anti-Inflammatory and Pro-Resolving Effects of Anabasum in a Human Model of Self-Resolving Acute Inflammation. Clinical Pharmacology and Therapeutics. 2018;104(4):675–686. https://doi.org/10.1002/cpt.980

25. Motwani MP, Flint JD, De Maeyer RPH, Fullerton JN, Smith AM, Marks DJB, Gilroy DW. Novel translational model of resolving inflammation triggered by UV-killed E. coli. Journal of Pathology: Clinical Research. 2016;2(3):154–165. https://doi.org/10.1002/cjp2.43

26. Wainwright M, Crossley KB. Methylene Blue - a Therapeutic Dye for All Seasons? Journal of Chemotherapy. 2002;14(5):431–443. https://doi.org/10.1179/joc.2002.14.5.431

27. Kayabaşı Y. Methylene blue and its importance in medicine. Demiroglu Science University Florence Nightingale Journal of Medicine. 2020;6(3):136–145. http://dx.doi.org/10.5606/fng.btd.2020.25035

28. Barbosa P, Peters TM. The effects of vital dyes on living organisms with special reference to Methylene Blue and Neutral Red. The Histochemical Journal. 1971;3(1):71–93. https://doi.org/10.1007/bf01686508

29. Liu X, Wu X, Yang J. Protein determination using methylene blue in a synchronous fluorescence technique. Talanta. 2010;81(3):760–765. https://doi.org/10.1016/j.talanta.2010.01.014

30. Pahang F, Parvin P, Ghafoori-Fard H, Bavali A, Moafi A. Fluorescence properties of methylene blue molecules coupled with metal oxide nanoparticles. OSA Continuum. 2020;3(3):688. https://doi.org/10.1364/OSAC.387557

31. Tchaikovskaya O, Chaidonova V, Bocharnikova E, Telminov E, Dmitrieva N, Ezhov D. Solvent effect on the Spectra of Methylene Green and Methylene Blue. Journal of Fluorescence. 2023;33(2):685–695. https://doi.org/10.1007/s10895-022-03074-2

32. Sturgis CC, Bethell FH. Quantitative and Qualitative Variations in Normal Leukocytes. Physiological Reviews. 1943;23(3):279–303. https://doi.org/10.1152/physrev.1943.23.3.279

33. Malawista SE. Cytochalasin B Reversibly Inhibits Phagocytosis by Human Blood Leukocytes. In: Progress in Immunology. Elsevier; 1971. p. 187–192. https://doi.org/10.1016/B978-0-12-057550-3.50021-1

34. Nowicka M, Krieg C, Crowell HL, Weber LM, Hartmann FJ, Guglietta S, Becher B, Levesque MP, Robinson MD. CyTOF workflow: differential discovery in high-throughput

high-dimensional cytometry datasets. F1000Research. 2019;6:748. https://doi.org/10.12688/f1000research.11622.3

35. Pushparajah Mak RS, Liebelt EL. Methylene Blue. Pediatric Emergency Care. 2021;37(9):474–477. https://doi.org/10.1097/pec.0000000000002526

36. Howland MA. Methylene blue. In: History of Modern Clinical Toxicology. Elsevier; 2022. p. 231–241. https://doi.org/10.1016/B978-0-12-822218-8.00052-1

37. Batth TS, Singh P, Ramakrishnan VR, Sousa MML, Chan LJG, Tran HM, Luning EG, Pan EHY, Vuu KM, Keasling JD, et al. A targeted proteomics toolkit for high-throughput absolute quantification of Escherichia coli proteins. Metabolic Engineering. 2014;26:48–56. https://doi.org/10.1016/j.ymben.2014.08.004

38. Viegas MS, Estronca LMBB, Vieira O V. Comparison of the Kinetics of Maturation of Phagosomes Containing Apoptotic Cells and IgG-Opsonized Particles Coers J, editor. PLoS ONE. 2012;7(10):e48391. https://doi.org/10.1371/journal.pone.0048391

39. Touret N, Paroutis P, Terebiznik M, Harrison RE, Trombetta S, Pypaert M, Chow A, Jiang A, Shaw J, Yip C, et al. Quantitative and Dynamic Assessment of the Contribution of the ER to Phagosome Formation. Cell. 2005;123(1):157–170. https://doi.org/10.1016/j.cell.2005.08.018

40. Furukawa A, Nakada-Tsukui K, Nozaki T. Novel Transmembrane Receptor Involved in Phagosome Transport of Lysozymes and β-Hexosaminidase in the Enteric Protozoan Entamoeba histolytica Johnson PJ, editor. PLoS Pathogens. 2012;8(2):e1002539. https://doi.org/10.1371/journal.ppat.1002539

41. Levin-Konigsberg R, Montaño-Rendón F, Keren-Kaplan T, Li R, Ego B, Mylvaganam S, DiCiccio JE, Trimble WS, Bassik MC, Bonifacino JS, et al. Phagolysosome resolution

requires contacts with the endoplasmic reticulum and phosphatidylinositol-4-phosphate signalling. Nature Cell Biology. 2019;21(10):1234–1247. https://doi.org/10.1038/s41556-019-0394-2

42. Harriff MJ, Burgdorf S, Kurts C, Wiertz EJHJ, Lewinsohn DA, Lewinsohn DM. TAP Mediates Import of Mycobacterium tuberculosis-Derived Peptides into Phagosomes and Facilitates Loading onto HLA-I Briken V, editor. PLoS ONE. 2013;8(11):e79571. https://doi.org/10.1371/journal.pone.0079571

43. Naish E, Wood AJ, Stewart AP, Routledge M, Morris AC, Chilvers ER, Lodge KM. The formation and function of the neutrophil phagosome. Immunological Reviews. 2023;314(1):158–180. https://doi.org/10.1111/imr.13173

44. Campos LC, Di Colo G, Dattani V, Braggins H, Kumararatne D, Williams AP, Alachkar H, Jolles S, Battersby A, Cole T, et al. Long-term outcomes for adults with chronic granulomatous disease in the United Kingdom. Journal of Allergy and Clinical Immunology. 2021;147(3):1104–1107. https://doi.org/10.1016/j.jaci.2020.08.034

45. Smith AM, Rahman FZ, Hayee B, Graham SJ, Marks DJB, Sewell GW, Palmer CD, Wilde J, Foxwell BMJ, Gloger IS, et al. Disordered macrophage cytokine secretion underlies impaired acute inflammation and bacterial clearance in Crohn's disease. Journal of Experimental Medicine. 2009;206(9):1883–1897. https://doi.org/10.1084/jem.20091233

46. Mellman IS, Plutner H, Steinman RM, Unkeless JC, Cohn ZA. Internalization and degradation of macrophage Fc receptors during receptor-mediated phagocytosis. The Journal of cell biology. 1983;96(3):887–895. https://doi.org/10.1083/jcb.96.3.887

47. Stow JL, Condon ND. The cell surface environment for pathogen recognition and entry. Clinical & Translational Immunology. 2016;5(4). https://doi.org/10.1038/cti.2016.15

48. Roberts CA, Buikstra JE. Bacterial Infections. In: Ortner's Identification of Pathological Conditions in Human Skeletal Remains. Elsevier; 2019. p. 321–439. https://doi.org/10.1016/B978-0-12-809738-0.00011-9

49. Doron S, Gorbach SL. Bacterial Infections: Overview. In: International Encyclopedia of Public Health. Elsevier; 2008. p. 273–282. https://doi.org/10.1016%2FB978-012373960-5.00596-7

50. Fiuza C, Salcedo M, Clemente G, Tellado JM. In vivo neutrophil dysfunction in cirrhotic patients with advanced liver disease. Journal of Infectious Diseases. 2000;182(2):526–533. https://doi.org/10.1086/315742

51. George S, Hamblin MR, Kishen A. Uptake pathways of anionic and cationic photosensitizers into bacteria. Photochemical & Photobiological Sciences. 2009;8(6):788–795. https://doi.org/10.1039/B809624D

52. McCalla TM. Cation Adsorption by Bacteria. Journal of Bacteriology. 1940;40(1):23–32. https://doi.org/10.1128/jb.40.1.23-32.1940

53. Sabbahi S, Ben Ayed L, Boudabbous A. Cationic, anionic and neutral dyes: effects of photosensitizing properties and experimental conditions on the photodynamic inactivation of pathogenic bacteria. Journal of Water and Health. 2013;11(4):590–599. https://doi.org/10.2166/wh.2013.219

54. Panda AK, Chakraborty AK. Studies on the interaction of bacterial lipopolysaccharide with cationic dyes by absorbance and fluorescence spectroscopy. Journal of

Photochemistry and Photobiology A: Chemistry. 1997;111(1–3):157–162. https://doi.org/10.1016/S1010-6030(97)00162-7

55. Usacheva MN, Teichert MC, Biel MA. The role of the methylene blue and toluidine blue monomers and dimers in the photoinactivation of bacteria. Journal of Photochemistry and Photobiology B: Biology. 2003;71(1–3):87–98. https://doi.org/10.1016/j.jphotobiol.2003.06.002

56. Marconi G, Quintana R. Methylene blue dyeing of cellular nuclei during salpingoscopy, a new in- vivo method to evaluate vitality of tubal epithelium. Human Reproduction. 1998;13(12):3414–3417. https://doi.org/10.1093/humrep/13.12.3414

57. Akram AR, Chankeshwara SV, Scholefield E, Aslam T, McDonald N, Megia-Fernandez A, Marshall A, Mills B, Avlonitis N, Craven TH, et al. In situ identification of Gram-negative bacteria in human lungs using a topical fluorescent peptide targeting lipid A. Science Translational Medicine. 2018;10(464):1–12. https://doi.org/10.1126/scitranslmed.aal0033

58. Akram AR, Avlonitis N, Lilienkampf A, Perez-Lopez AM, McDonald N, Chankeshwara S V., Scholefield E, Haslett C, Bradley M, Dhaliwal K. A labelled-ubiquicidin antimicrobial peptide for immediate in situ optical detection of live bacteria in human alveolar lung tissue. Chemical Science. 2015;6(12):6971–6979. https://doi.org/10.1039/c5sc00960j

59. Paulsson JM, Jacobson SH, Lundahl J. Neutrophil activation during transmigration in vivo and in vitro. A translational study using the skin chamber model. Journal of Immunological Methods. 2010;361(1–2):82–88. https://doi.org/10.1016/j.jim.2010.07.015

60. Sengeløv H, Follin P, Kjeldsen L, Lollike K, Dahlgren C, Borregaard N. Mobilization of granules and secretory vesicles during in vivo exudation of human neutrophils. The

Journal of Immunology. 1995;154(8):4157–4165. https://doi.org/10.4049/jimmunol.154.8.4157

61. Paulsson J, Dadfar E, Held C, Jacobson SH, Lundahl J. Activation of peripheral and in vivo transmigrated neutrophils in patients with stable coronary artery disease. Atherosclerosis. 2007;192(2):328–334. https://doi.org/10.1016/j.atherosclerosis.2006.08.003

62. Davidsson L, Rudin AD, Klose FPS, Buck A, Björkman L, Christenson K, Bylund J. In vivo transmigrated human neutrophils are highly primed for intracellular radical production induced by monosodium urate crystals. International Journal of Molecular Sciences. 2020;21(11). https://doi.org/10.3390/ijms21113750

63. Margraf A, Ley K, Zarbock A. Neutrophil Recruitment: From Model Systems to Tissue-Specific Patterns. Trends in immunology. 2019;40(7):613–634. https://doi.org/10.1016/j.it.2019.04.010

64. Di A, Brown ME, Deriy L V., Li C, Szeto FL, Chen Y, Huang P, Tong J, Naren AP, Bindokas V, et al. CFTR regulates phagosome acidification in macrophages and alters bactericidal activity. Nature Cell Biology. 2006;8(9):933–944. https://doi.org/10.1038/ncb1456

65. Belhoussine R, Morjani H, Sharonov S, Ploton D, Manfait M. Characterization of intracellular pH gradients in human multidrug- resistant tumor cells by means of scanning microspectrofluorometry and dual- emission-ratio probes. International Journal of Cancer. 1999;81(1):81–89. https://doi.org/10.1002/(sici)1097-0215(19990331)81:1%3C81::aid-ijc15%3E3.0.co;2-p

66. Matsui A, Tanaka E, Soo Choi H, Kianzad V, Gioux S, Lomnes SJ, Frangioni J V. Real-time, near-infrared, fluorescence-guided identification of the ureters using methylene blue. https://doi.org/10.1016/j.surg.2009.12.003

67. Hemdan SS. The Shift in the Behavior of Methylene Blue Toward the Sensitivity of Medium: Solvatochromism, Solvent Parameters, Regression Analysis and Investigation of Cosolvent on the Acidity Constants. Journal of Fluorescence. https://doi.org/10.1007/s10895-023-03234-y

68. Vuggili SB, Gaur UK, Tyagi T, Sharma M. 2D/2D nitrogen-doped graphitic carbon nitride/cobalt sulfide nanostructures for fast photodegradation of methylene blue dye and real industrial sewage effluents. Environmental Science: Advances. 2023;2(5):795–814. https://doi.org/10.1039/d2va00208f

69. Wang Y, Shi R, Lin J, Zhu Y. Significant photocatalytic enhancement in methylene blue degradation of TiO2 photocatalysts via graphene-like carbon in situ hybridization. Applied Catalysis B: Environmental. 2010;100(1–2):179–183. https://doi.org/10.1016/j.apcatb.2010.07.028

70. Khan I, Saeed K, Zekker I, Zhang B, Hendi AH, Ahmad A, Ahmad S, Zada N, Ahmad H, Shah LA, et al. Review on Methylene Blue: Its Properties, Uses, Toxicity and Photodegradation. Water (Switzerland). 2022;14(2). https://doi.org/10.3390/w14020242

71. Felgenträger A, Maisch T, Dobler D, Späth A. Hydrogen bond acceptors and additional cationic charges in methylene blue derivatives: Photophysics and antimicrobial efficiency. BioMed Research International. 2013;2013. https://doi.org/10.1155/2013/482167

72. Siong VLE, Lee KM, Juan JC, Lai CW, Tai XH, Khe CS. Removal of methylene blue dye by solvothermally reduced graphene oxide: A metal-free adsorption and

photodegradation method. RSC Advances. 2019;9(64):37686–37695. https://doi.org/10.1039/C9RA05793E

73. Leliefeld PHC, Pillay J, Vrisekoop N, Heeres M, Tak T, Kox M, Rooijakkers SHM, Kuijpers TW, Pickkers P, Leenen LPH, et al. Differential antibacterial control by neutrophil subsets. Blood Advances. 2018;2(11):1344–1354. https://doi.org/10.1182/bloodadvances.2017015578

74. Perrenoud L, Conley J, Berg LJ. Analysis of T-cell Receptor-Induced Calcium Influx in Primary Murine T-cells by Full Spectrum Flow Cytometry. Journal of Visualized Experiments. 2022;2022(190):1–18. https://doi.org/10.3791/64526

75. Henderson J, Havranek O, Ma MCJ, Herman V, Kupcova K, Chrbolkova T, Pacheco-Blanco M, Wang Z, Comer JM, Zal T, et al. Detecting Förster resonance energy transfer in living cells by conventional and spectral flow cytometry. Cytometry Part A. 2022;101(10):818–834. https://doi.org/10.1002/cyto.a.24472

76. Lim JW, Petersen M, Bunz M, Simon C, Schindler M. Flow cytometry based-FRET: basics, novel developments and future perspectives. Cellular and Molecular Life Sciences. 2022;79(4):1–12. https://doi.org/10.1007/s00018-022-04232-2

77. Trevisan E, Menegazzi R, Zabucchi G, Troian B, Prato S, Vita F, Rapozzi V, Grandolfo M, Borelli V. Effect of methylene blue photodynamic therapy on human neutrophil functional responses. Journal of Photochemistry and Photobiology B: Biology. 2019;199(August):111605. https://doi.org/10.1016/j.jphotobiol.2019.111605

78. Lin ZH, Wang SY, Chen LL, Zhuang JY, Ke QF, Xiao DR, Lin WP. Methylene blue mitigates acute neuroinflammation after spinal cord injury through inhibiting NLRP3

inflammasome activation in microglia. Frontiers in Cellular Neuroscience. 2017;11(December):1–13. https://doi.org/10.3389/fncel.2017.00391

79. Tian ZG, Ji Y, Yan WJ, Xu CY, Kong CY, Han F, Zhao Y, Pang QF. Methylene blue protects against paraquat-induced acute lung injury in rats. International Immunopharmacology. 2013;17(2):309–313. https://doi.org/10.1016/j.intimp.2013.06.022

80. Galili Y, Ben-Abraham R, Weinbroum A, Marmur S, Iaina A, Volman Y, Peer G, Szold O, Soffer D, Klausner J, et al. Methylene Blue Prevents Pulmonary Injury after Intestinal Ischemia-Reperfusion. The Journal of Trauma: Injury, Infection, and Critical Care. 1998;45(2):222–226. https://doi.org/10.1097/00005373-199808000-00004

81. Nordenfelt P, Tapper H. Phagosome dynamics during phagocytosis by neutrophils. Journal of Leukocyte Biology. 2011;90(2):271–284. https://doi.org/10.1189/jlb.0810457

82. Segal AW, Geisow M, Garcia R, Harper A, Miller R. The respiratory burst of phagocytic cells is associated with a rise in vacuolar pH. Nature. 1981;290(5805):406–409. https://doi.org/10.1038/290406a0

83. Johansson A, Jesaitis AJ, Lundqvist H, Magnusson K-E, Sjölin C, Karlsson A, Dahlgren C. Different Subcellular Localization of Cytochrome b and the Dormant NADPH-Oxidase in Neutrophils and Macrophages: Effect on the Production of Reactive Oxygen Species during Phagocytosis. Cellular Immunology. 1995;161(1):61–71. https://doi.org/10.1006/cimm.1995.1009

84. Jankowski A, Scott CC, Grinstein S. Determinants of the Phagosomal pH in Neutrophils. Journal of Biological Chemistry. 2002;277(8):6059–6066. https://doi.org/10.1074/jbc.m110059200

85. Macallan D. Infection and malnutrition. Medicine. 2009;37(10):525–528. https://doi.org/10.1016/j.mpmed.2009.07.005

86. Offner PJ. Male Gender Is a Risk Factor for Major Infections After Surgery. Archives of Surgery. 1999;134(9):935. https://doi.org/10.1001/archsurg.134.9.935

87. Zhu X, Herrera G, Ochoa JB. Immunosupression and Infection After Major Surgery: A Nutritional Deficiency. Critical Care Clinics. 2010;26(3):491–500. https://doi.org/10.1016/j.ccc.2010.04.004

88. Klein NC, Go CHU, Cunha BA. Infections associated with steroid use. Infectious Disease Clinics of North America. 2001;15(2):423–432. https://doi.org/10.1016/s0891-5520(05)70154-9

89. Thomas PA. Unexplained Immunodeficiency in Children. JAMA. 1984;252(5):639. https://doi.org/10.1001/jama.1984.03350050027021

90. Reinhart MB, Huntington CR, Blair LJ, Heniford BT, Augenstein VA. Indocyanine Green. Surgical Innovation. 2016;23(2):166–175. https://doi.org/10.1177/1553350615604053

91. Mordon S, Devoisselle JM, Soulie-Begu S, Desmettre T. Indocyanine Green: Physicochemical Factors Affecting Its Fluorescencein Vivo. Microvascular Research. 1998;55(2):146–152. https://doi.org/10.1006/mvre.1998.2068

92. Piorecka K, Kurjata J, Stanczyk WA. Acriflavine, an Acridine Derivative for Biomedical Application: Current State of the Art. Journal of Medicinal Chemistry. 2022;65(17):11415–11432. https://doi.org/10.1021/acs.jmedchem.2c00573

93. Xie X, Shi Q, Wu P, Zhang X, Kambara H, Su J, Yu H, Park SY, Guo R, Ren Q, et al. Single-cell transcriptome profiling reveals neutrophil heterogeneity in homeostasis and

infection. Nature Immunology. 2020;21(9):1119–1133. https://doi.org/10.1038/s41590-020-0736-z

94. Adrover JM, del Fresno C, Crainiciuc G, Cuartero MI, Casanova-Acebes M, Weiss LA, Huerga-Encabo H, Silvestre-Roig C, Rossaint J, Cossío I, et al. A Neutrophil Timer Coordinates Immune Defense and Vascular Protection. Immunity. 2019;50(2):390-402.e10. https://doi.org/10.1016/j.immuni.2019.01.002

95. Casanova-Acebes M, Nicolás-Ávila JA, Li JL, García-Silva S, Balachander A, Rubio-Ponce A, Weiss LA, Adrover JM, Burrows K, A-González N, et al. Neutrophils instruct homeostatic and pathological states in naive tissues. Journal of Experimental Medicine. 2018;215(11):2778–2795. https://doi.org/10.1084/jem.20181468

10. Figure legends

Figure 1

Chemical structure of methylene blue (*methylthioninium chloride*).

Figure 2

Optimising MB detection by flow cytometry and fluorescence microscopy. (A) Absorbance spectra of 4 concentrations of MB detected by spectrophotometry. **(B)** Emission spectra of 1% MB after excitation by 4 fluorescence microscopy lasers using the *Leica TCS SP8* HyD detector. **(C)** Emission spectra of MB-labelled leucocytes after excitation by 5 spectral flow cytometry lasers, with the 637nm detector set sensitivity increased to 70 and all values normalised so that the peak equals 1. **(D)** Representative Cytospin™ of MB-labelled leucocytes, as detected by fluorescence microscopy after red

laser excitation. **(E)** MFI of MB-labelled leucocytes in all conventional flow cytometry channels at the default detector voltages, in rank order of MFI (n=3). **(F)** Ribbon plot showing emission spectrum of MB alongside 16 conjugated antibody fluorophores, after excitation by all 5 spectral flow cytometry lasers. BV = brilliant violet, BUV = brilliant ultraviolet, FITC = fluorescein isothiocyanate, MB = methylene blue, MFI = (geometric) mean fluorescence intensity, PacBlue = pacific blue, PE = phycoerythrin, SB = spark blue, SV = spark violet, SYG = spark yellow green.

Figure 3

Labelling, washing, and quantifying methylene blue-labelled *E. coli*. (A) Fall in MB concentration between the *E. coli* labelling, washing, and final resuspension solutions during the process of labelling UV-killed *E. coli* with MB to produce MBEC (n=5). **(B)** Representative spectral flow cytometry plots of unlabelled *E. coli* (left) and MBEC (right), showing SSC (Y-axis) and MB fluorescence values (X-axis). **(C)** MB MFI of MBEC compared to MB-inert compensation beads suspended in the same supernatants (n=3). **(D)** MB MFI of MBEC during a 3-hour incubation in RPMI + 10% FCS at 37°C (n=3). **(E)** Increasing quantities (i.e. CFUs) of *E. coli* were labelled with 1.3µL of 1% MB and the absorption of MB by the *E. coli* was inferred from the concentration of MB remaining in the washing solutions after MB-labelling and resuspension in PBS, using the formula: mass = concentration x volume (n=3). **(F)** Optical density growth curve of unlabelled *E. coli* using 420nm light. **(G)** Absorbance spectrum of unlabelled *E. coli* (n=3). Significance reported using a paired Student's t-test (C) or one-way ANOVA with Dunnett's multiple comparisons test (A, D). ns = not significant, ****$p \leq 0.0001$. CFU = colony forming units,

MB = methylene blue, MBEC = methylene blue-labelled *E. coli*, MFI = (geometric) mean fluorescence intensity, OD = optical density, SSC = side scatter, UV = ultraviolet.

Figure 4

***Ex vivo* co-culture of methylene blue-labelled *E. coli* with human circulating leucocytes. (A)** MB MFI of circulating leucocyte subsets after 60min MBEC co-culture (n=3, MOI = 30). **(B)** MB MFI of isolated neutrophils at different time-points during 60min MBEC co-culture (n=3, MOI = 10). **(C)** MB MFI of isolated neutrophils after 60min MBEC co-culture at increasing MOI (n=3). **(D)** MB MFI of isolated neutrophils after 60min co-culture with MBEC or unlabelled *E. coli*, with or without pre-treatment with 10μM cytochalasin B to inhibit phagocytosis (n=3, MOI = 30).[33] **(E)** Fold change MB MFI during MBEC co-culture with monocyte-derived macrophages or naïve circulating monocytes, calculated as fold change from control cells without bacteria (n=3, MOI = 100). **(F)** Fluorescence microscopy of circulating leucocytes after 60min MBEC co-culture (MOI = 40, *Leica TCS SP8*). **(G)** Fluorescence microscopy of cellular distribution of MB^{hi} cellular inclusions in 4 leucocyte subsets after 60min co-culture of circulating leucocytes with unlabelled *E. coli* (left) or MBEC (right, MOI = 30). **(H)** Still frames from a representative live imaging video (Supplemental Data 2) of isolated neutrophils co-cultured with unlabelled *E. coli* (left) or MBEC (right) for 20min during real-time DIC and fluorescence imaging microscopy (MOI = 100, *Zeiss LSM980 Airyscan*). **(I)** Effect of cell membrane permeabilisation buffer treatment on neutrophil MB MFI after 60min MBEC co-culture (n=3, MOI = 30), calculated as the fold change from control neutrophils without MBEC. **(J)** MFI fold-change of pHrodo™ green or MB during co-culture of neutrophils from

healthy volunteers with pHrodo™ green *E. coli* BioParticles or MBEC, respectively (n=3, MOI = 20), calculated as the fold change from control neutrophils without bacteria. Significance reported using a paired Student's *t*-test (H) or one-way ANOVA with Dunnett's multiple comparisons test (A, B, C, D, E). ns = not significant, $^{**}p \leq 0.01$, $^{***}p \leq 0.001$, $^{****}p \leq 0.0001$. CytB = cytochalasin B, DIC = differential interference contrast, FITC = fluorescein isothiocyanate, MB = methylene blue, MBEC = methylene blue-labelled E. coli, MFI = (geometric) mean fluorescence intensity, MOI = multiplicity of infection, NK = natural killer, VEH = vehicle.

Figure 5

'Red shift' in methylene blue fluorescence during *ex vivo* MBEC phagocytosis. (A) Neutrophil MB MFI in the 3 red-excited red-emitting conventional flow cytometry channels (AF647, AF700, and APC-Cy7) at above default detector voltages (AF647 = 650, AF700 = 650, APC-Cy7 = 600) during *ex vivo* MBEC co-culture (MOI = 10). This included the merged 'MB channel', where data from all 3 channels were combined *post hoc* using FCS Express™ software (n=3). **(B)** Representative conventional flow cytometry compensation matrix when MB was detected alongside 13 conjugated antibody fluorophores (Supplemental Data 1, overlap values of >40% highlighted). **(C)** Comparison of neutrophil MB MFI using the AF647 (near-red) and APC-Cy7 (far-red) channels during *ex vivo* MBEC co-culture (n=3). **(D)** Data in (C) presented as the far-to-near-red (i.e. APC-Cy7 : AF647) channel ratio. **(E)** Neutrophil MB emission spectra during *ex vivo* MBEC co-culture analysed by spectral flow cytometry and corrected for total MB MFI at each time-point by dividing each data point by the sum of all data points for each time-point, to allow for side-

by-side comparison of MB emission spectra over time (MOI = 20). **(F, G)** Absorbance (F) and emission (G) spectra of MB when combined *in vitro* with increasing concentrations of hydrogen peroxide (H_2O_2). **(H, I)** Effect of gp91phox chronic granulomatous disease status on neutrophil MB MFI (H) and neutrophil APC-Cy7 : AF647 channel ratio (I) during *ex vivo* neutrophil MBEC co-culture (n=4). **(J)** Data from the 180min time-point in (I) analysed using spectral flow cytometry. **(K)** Effect of *E. coli* MB labelling concentration on neutrophil MB 'red shift' (APC-Cy7:AF647 ratio) during *ex vivo* neutrophil MBEC co-culture (n=3). Significance reported using a paired Student's *t*-test (C), one-way ANOVA with Dunnett's multiple comparisons test (D), or two-way ANOVA with Tukey's multiple comparisons test (H & I, comparing unaffected vs affected, and K comparing 0.3% to 1% MB). ns = not significant, *$p \leq 0.05$, **$p \leq 0.01$, ***$p \leq 0.001$, ****$p \leq 0.0001$. APC-Cy7 = Allophycocyanin-Cyanine 7, AF = AlexaFluor, MB = methylene blue, MFI = (geometric) mean fluorescence intensity.

Figure 6

Effect of methylene blue on the immune response in humans. (A-D) Surface membrane expression of CD11b **(A)**, CD45 **(B)**, CD62L **(C)**, and CD66b **(D)** on neutrophils during *ex vivo* co-culture with unlabelled *E. coli* or MBEC (n = 19, MOI = 5) in RPMI + 10% FCS. **(E-F)** Effect of MB (E) or MBEC (F) concentration on *ex vivo* neutrophil phagocytosis of pHrodo™ green *E.* coli BioParticles (n=3). **(G)** Comparison of dermal vascular hyperaemia between intradermal unlabelled *E. coli* or MBEC injections in healthy volunteers, measured by laser doppler blood flow imaging. **(H)** Representative skin biopsy

sections comparing dermal CD66b^{hi} neutrophil infiltration over time after intradermal unlabelled *E. coli* or MBEC injections in healthy volunteers imaged using fluorescence microscopy (see Supplemental Data 3B for Hoechst counterstaining). **(I-K)** Effect of intradermal MBEC injection on dermal vascular hyperaemia (I), relative dermal leucocyte abundance (J), and absolute circulating leucocyte abundance (K) in healthy volunteers (n=6) (see Supplemental Data 3C for absolute blister leucocyte abundances). Significance reported using paired Student's *t*-tests (A-D, F) or one-way ANOVAs with Dunnett's multiple comparisons test (E, I). ns = not significant, *$p \leq 0.05$, **$p \leq 0.01$, ****$p \leq 0.0001$. FITC = fluorescein isothiocyanate, MB = methylene blue, MBEC = methylene blue-labelled *E. coli*, MOI = multiplicity of infection, NK = natural killer.

Figure 7

Neutrophil responses 2-3h after intradermal MBEC injection in healthy volunteers. **(A-C)** UMAP (A), heatmap (B) and MB fluorescence (C) of blood and blister neutrophils sampled 2-3h after intradermal injection of $3x10^7$ CFU MBEC in healthy volunteers (n=7). **(D-F)** MB fluorescence (D), UMAP (E), and heatmap (F) of blister neutrophils sampled 2-3h after the intradermal injection of $3x10^7$ CFU MBEC in healthy volunteers (n=7). CXCR = chemokine (C-X-C motif) receptor, MB = methylene blue, MBEC = methylene blue-labelled *E. coli*, Siglec = sialic-acid-binding immunoglobulin-like lectin, UMAP = uniform manifold approximation and projection.

Figure 8

Neutrophil responses 3-24h after intradermal MBEC injection in healthy volunteers. **(A-C)** UMAP (A), MB fluorescence (B) and heatmap (C) of blood and blister neutrophils sampled 3-24h after intradermal injection of $6x10^7$ CFU MBEC in healthy volunteers (n=19). **(D)** Red emission spectra of MB^{hi} blister neutrophils measured by spectral flow cytometry 3-24h after intradermal injection of $6x10^7$ CFU MBEC in healthy volunteers (n=19, 7/8 samples per time-point). **(E, F)** MB MFI of blood and blister neutrophils (E) and MB^{hi} blister neutrophil counts (F) 3-24h after intradermal injection of $6x10^7$ CFU MBEC in healthy volunteers (n=19, 7/8 samples per time-point). **(G)** MB fluorescence intensity (MB MFI x cell count) of blister neutrophils (red, left Y-axis) and blister fluid endotoxin levels (black, right Y-axis) from suction blisters raised 3-24h after intradermal injection of $6x10^7$ MBEC CFU in healthy volunteers (n=19, 7/8 samples per time-point). **(H)** Correlations between MB and cell surface markers in blood and blister neutrophils sampled after *in vivo* intradermal MBEC injection ('*in vivo*') and after *ex vivo* MBEC phagocytosis assays using circulating neutrophils ('*ex vivo'*) in healthy volunteers (n=19). **(I)** Red emission spectra of MB^{hi} circulating neutrophils after a 45min *ex vivo* MBEC phagocytosis assay, and of MB^{hi} blister neutrophils 3-24h after intradermal injection of $6x10^7$ CFU MBEC in healthy volunteers, analysed by spectral flow cytometry. Data were corrected for total MB MFI at each time-point to allow for side-by-side comparison of neutrophil MB emission spectra between conditions. Significance reported using one-way ANOVA with Dunnett's multiple comparisons test (E, F). ns = not significant, $^{**}p \leq 0.01$, $^{****}p \leq 0.0001$. CCR = c-c motif receptor, CD = cluster of differentiation, CXCR = chemokine (C-X-C motif) receptor, MB = methylene blue, MBEC = methylene blue-labelled *E. coli*, MFI =

(geometric) mean fluorescence intensity, Siglec = sialic-acid-binding immunoglobulin-like lectin, UMAP = uniform manifold approximation and projection.

Figure 9

Leucocyte responses 3-24h after intradermal MBEC injection in healthy volunteers. **(A-C)** UMAP (A), MB fluorescence (B) and heatmap (C) of blood and blister leucocytes (excluding Siglec8^{hi} eosinophils) sampled 3-24h after intradermal injection of 6x10^{7} CFU MBEC in healthy volunteers (n=19). MB = methylene blue, MBEC = methylene blue-labelled *E. coli*, UMAP = uniform manifold approximation and projection.

ENDS

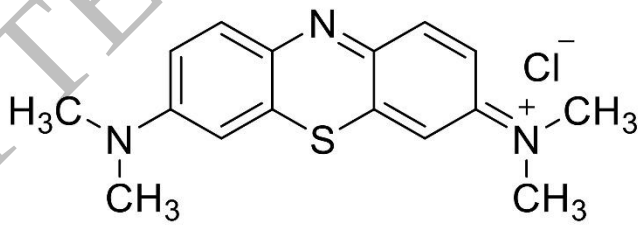

Figure 1
87x32 mm (DPI)

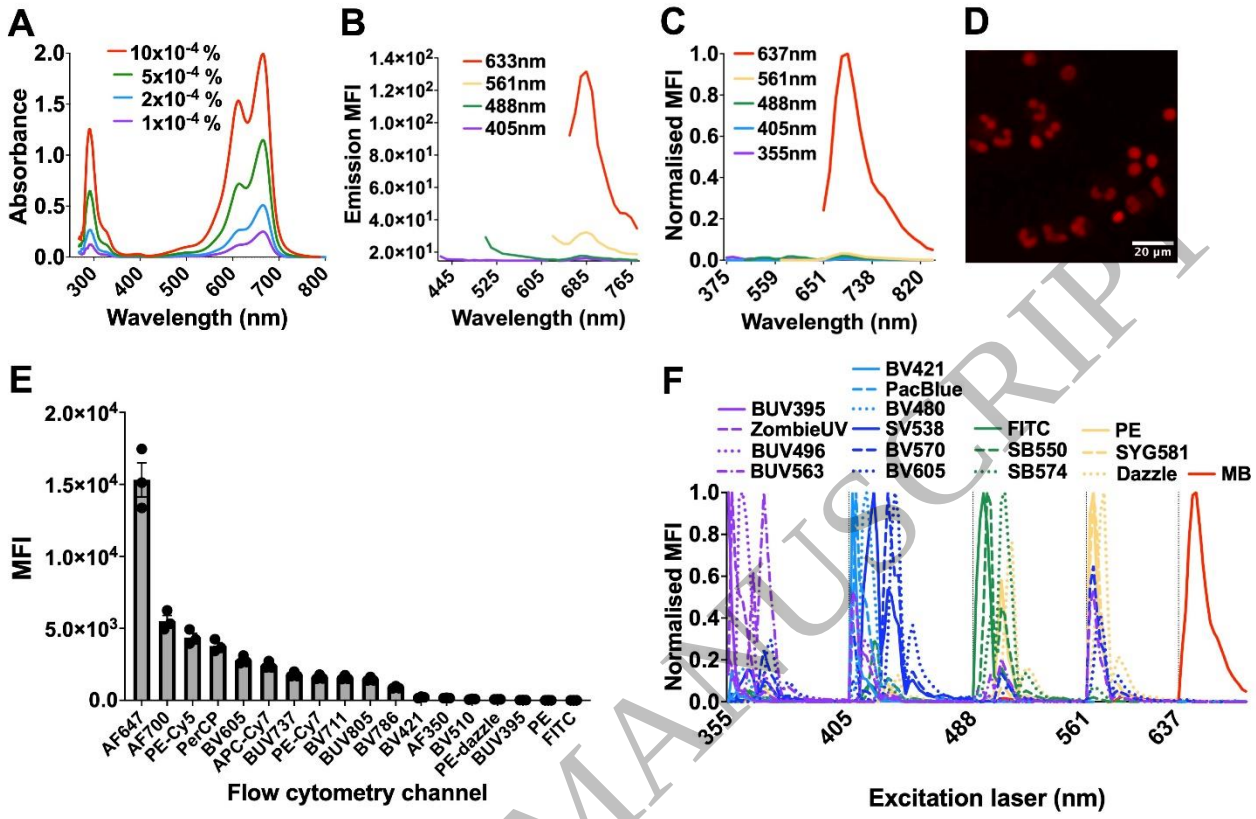

Figure 2
171x112 mm (DPI)

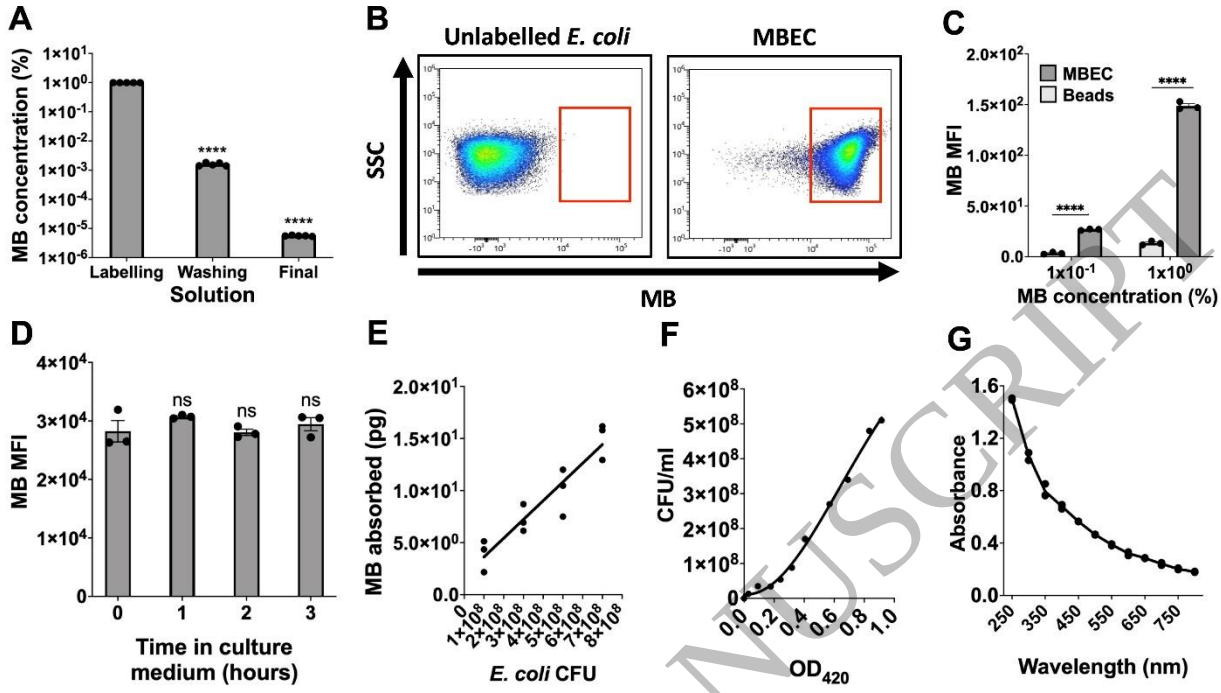

Figure 3
186x106 mm (DPI)

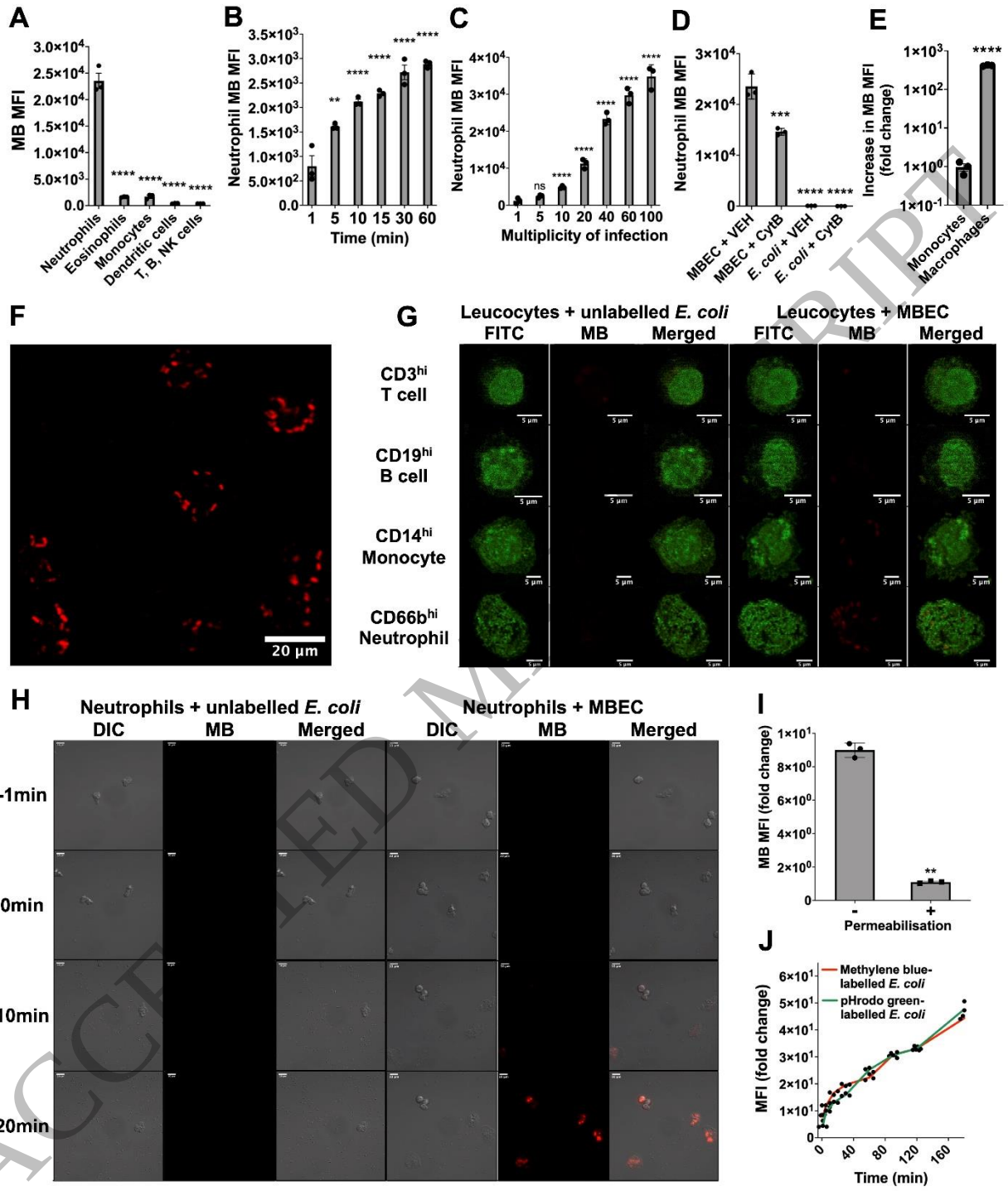

Figure 4
182x212 mm (DPI)

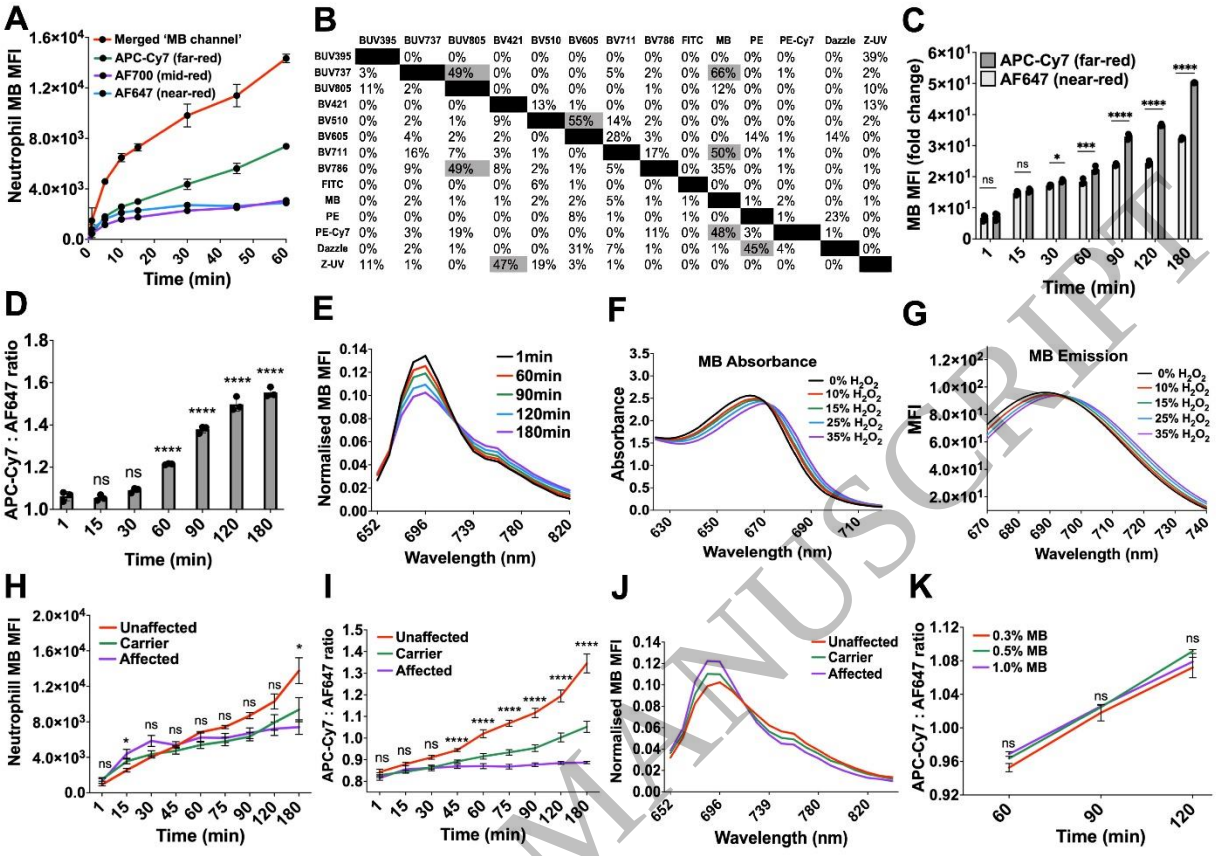

Figure 5
183x128 mm (DPI)

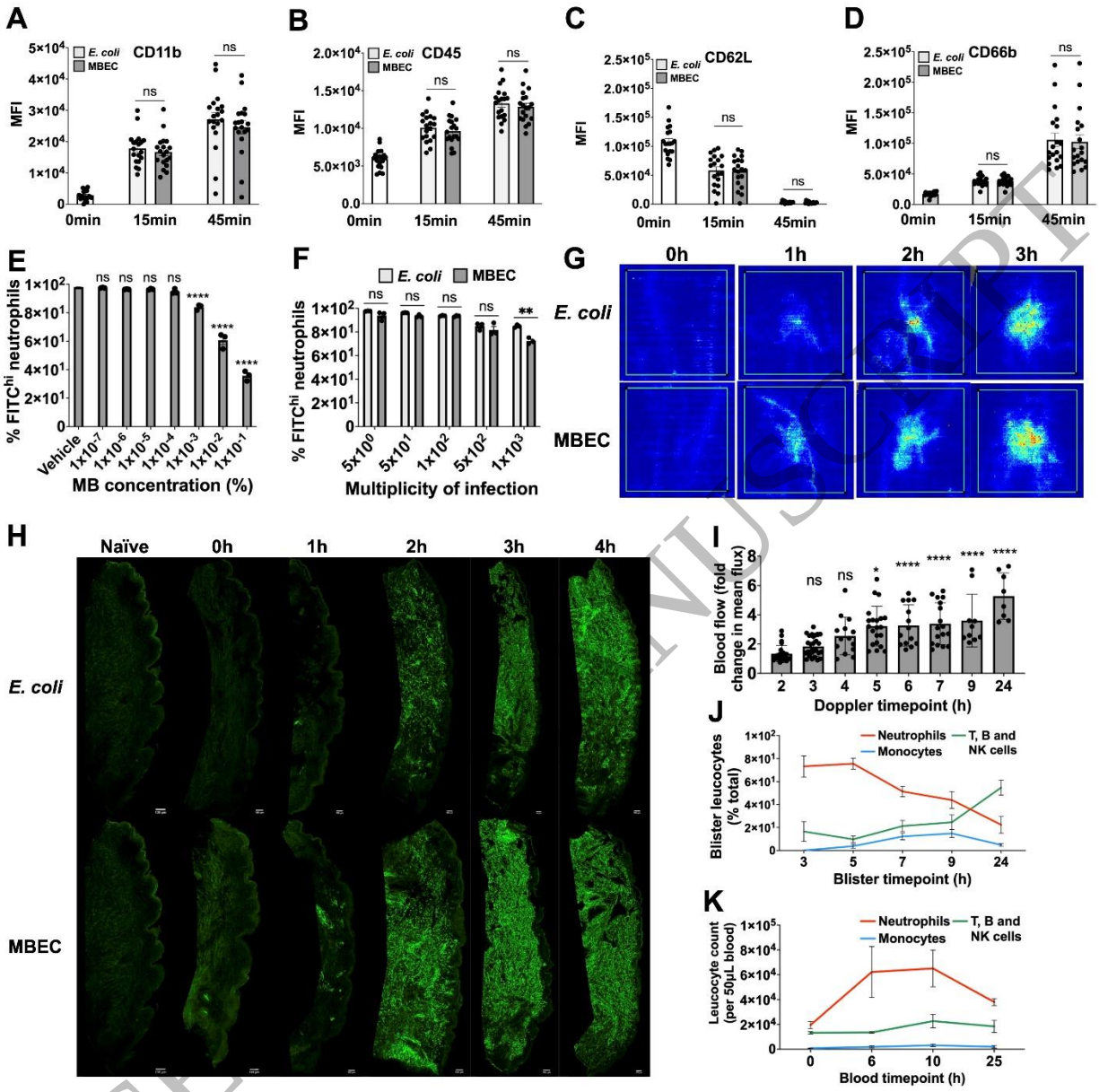

Figure 6
187x184 mm (DPI)

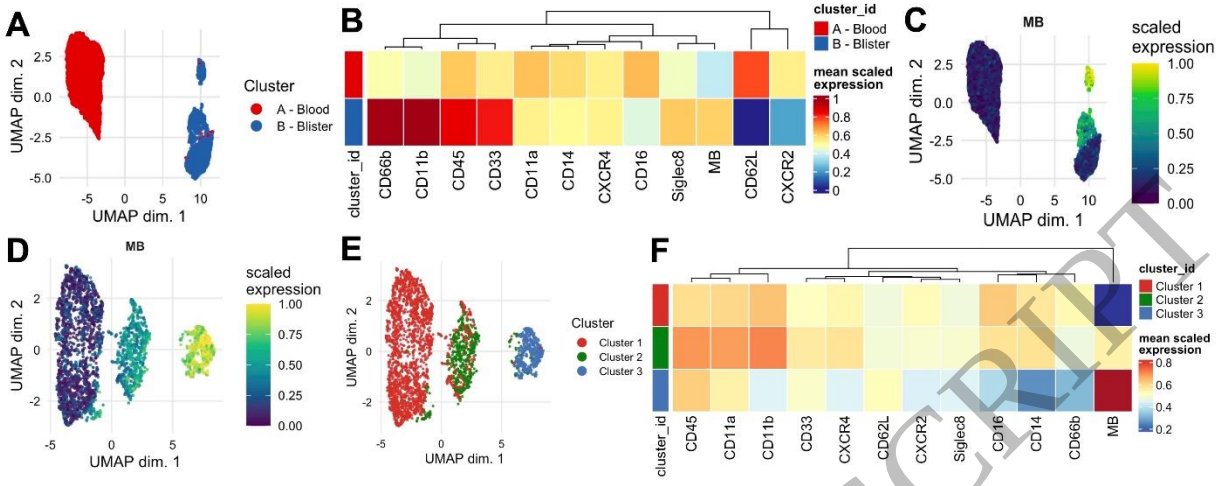

Figure 7
184x74 mm (DPI)

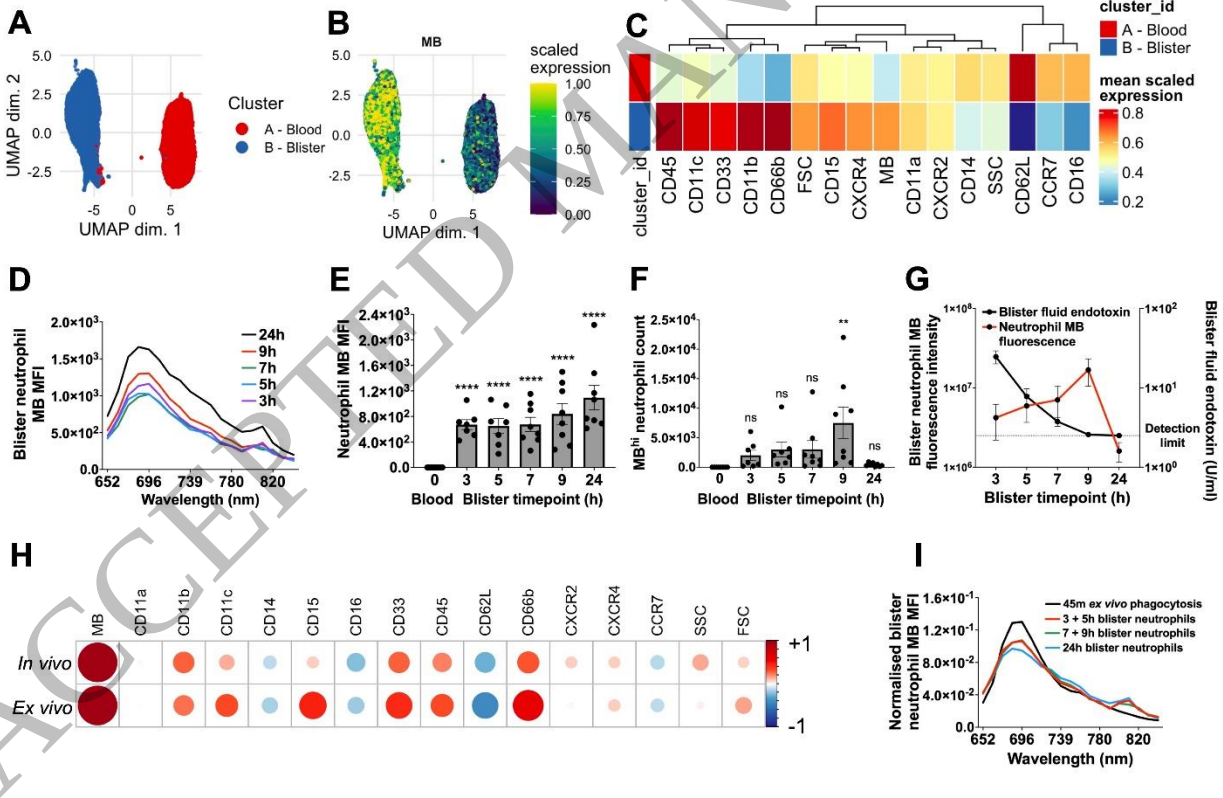

Figure 8
188x119 mm (DPI)

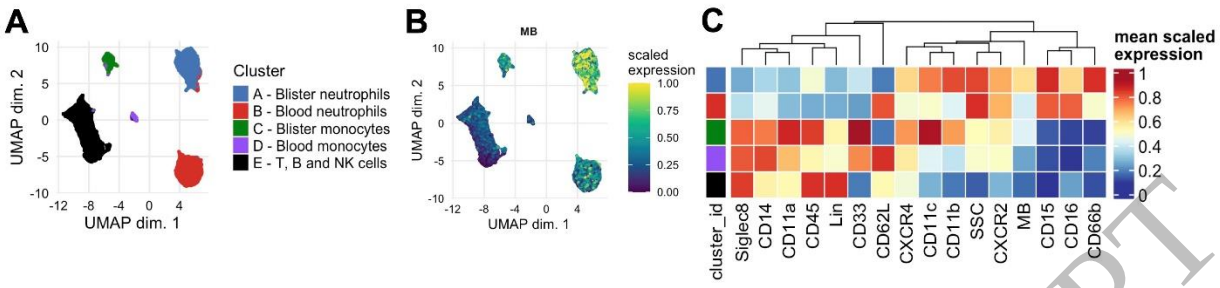

Figure 9
186x46 mm (DPI)